MATHEMATICAL MODEL OF DIFFERENTIAL REFLECTOMETRY FOR USE IN THE INVESTIGATION OF THIN FILM CORROSION PRODUCTS

By

FRANK KARL URBAN III

A DISSERTATION PRESENTED TO THE GRADUATE COUNCIL OF
THE UNIVERSITY OF FLORIDA
IN PARTIAL FULFILLMENT OF THE REQUIREMENTS FOR THE
DEGREE OF DOCTOR OF PHILOSOPHY

UNIVERSITY OF FLORIDA

1981

Bound by DOBBS BROS. LIBRARY BINDING CO., INC., St. Augustine, Florida

ACKNOWLEDGEMENTS

The author wishes to express his most sincere appreciation to his advisor, Dr. R. E. Hummel, for his long hours of assistance, patience and reverence for high ideals. Thanks especially to Dr. E. D. Verink, Jr. for support, encouragement and faith. Special thanks are also due Dr. R. T. DeHoff for encouragement and help above the call of duty. Dr. J. R. Ambrose, Dr. P. H. Holloway and Dr. G. Schmid were of much help in the performance of this work.

Thanks also to the many people who supported me during this effort including my family and friends. Also the support of the National Science Foundation is gratefully acknowledged.

TABLE OF CONTENTS

		PAGE
ACKNOWLEDGEMENTS		ii
ABSTRACT		v
SECTION		
I	INTRODUCTION	1
II	LITERATURE REVIEW	9
II-1	Introduction	9
II-2	General Theory of Optical Properties of Materials	9
II-3	Techniques for Bulk Optical Properties	11
II-4	Techniques for Absorbing Films	13
II-5	Techniques for Non-absorbing Films	17
II-6	Non-uniform Films	18
II-7	Metal Oxides	20
II-8	Optical Properties	21
II-9	Phase Diagrams	32
II-10	Electronic Structure	33
III	EXPERIMENTAL PROCEDURE	39
III-1	Introduction	39
III-2	Sample Preparation	39
III-3	Corrosion	42
III-4	Half-polishing	45
III-5	The Differential Reflectometer	47
III-6	Summary	50
IV	RESULTS AND DISCUSSION	51
IV-1	Introduction	51
IV-2	Model Geometry	51
IV-3	Interaction Between Light and Matter	53
IV-4	Computer Program	62
IV-5	Simplification of Equations	64
IV-6	Conceptualization of the Simplified Equation	65
IV-7	Results of the Calculations	69
IV-8	Calculated Differential Reflectograms, Thickness Effects	70
IV-9	Effect of n_1 Variation	77
IV-10	Effect of k_1 Variation	80

IV-11 Spectral Range Without Interference Peaks..... 83
IV-12 Interference Peak Shapes..... 87
IV-13 Theoretical Reflectogram Summary..... 90
IV-14 Tungsten Oxide..... 90
IV-15 Interband Transition Peaks..... 95
IV-16 Obtaining k and d..... 103
IV-17 Effect of Film Thickness on Signal Strength, R/R..... 106
IV-18 Effect of External Medium Variation.. 117
IV-19 Practical Aspects..... 119

V CONCLUSIONS AND SUGGESTIONS FOR FUTURE WORK.. 123
V-1 Conclusions..... 123
V-2 Suggestions for Future Work..... 124

APPENDICES

A COMPUTER MODEL DERIVATIONS..... 126
A-1 Transmission and Reflection Coefficients..... 126
A-2 Impedance in Terms of Optical Parameters..... 128
A-3 Attenuation Coefficients..... 130
A-4 Simplification of Master Equation.... 131

B MULTIPLE INTERNAL REFLECTION EQUATION..... 139
B-1 Derivation of Equation..... 139
B-2 Comparison of Multiple and Single Reflection Models..... 144
B-3 Multiple Internal Reflection Computer Program..... 144

C DIFFERENCE IN THICKNESS..... 146

D SINGLE INTERNAL REFLECTION PROGRAM..... 154

E PROGRAM FUNCTION..... 157

F THICKNESS FROM PEAK POSITION..... 159

REFERENCES..... 161

BIOGRAPHICAL SKETCH..... 165

Abstract of Dissertation Presented to the Graduate Council of the University of Florida in Partial Fulfillment of the Requirements of the Degree of Doctor of Philosophy

MATHEMATICAL MODEL OF DIFFERENTIAL REFLECTOMETRY FOR USE IN THE INVESTIGATION OF THIN FILM CORROSION PRODUCTS

By

Frank Karl Urban, III

March, 1981

Chairman: Rolf E. Hummel

Major Department: Materials Science and Engineering

A mathematical model dealing with the interaction of light with thin corrosion product films on metal substrates was developed. This model is different from previous models because it is based on Maxwell's equations only, utilizing no simplifying assumptions.

The model was developed to produce computer calculated differential reflectograms (difference in reflectivity as a function of photon energy) which were compared with experimentally obtained reflectograms. The calculated differential reflectograms are distinguished by a sequence of interference peaks if the product of film thickness and index of refraction of the corrosion product film is greater than 40 nanometers. For an oxide film thickness below this critical value, no interference peaks are

expected. The peaks obtained experimentally for these thin films are therefore caused by electron interband transitions. They can be used to identify specific metal oxides on metal substrates.

The computer model was tested by comparing the calculated differential reflectograms with experimental reflectograms of a number of oxides of various thicknesses grown on metal substrates by heating in dry oxygen. Specimens were prepared as follows. The oxide on half of the specimen surface was removed by mechanical polishing. The other half of the specimen was unaltered. The resulting reflectograms provide information based on the difference in reflectance between pure metal and corrosion product on metal substrates. High purity tungsten was chosen for the primary experimental thrust. Chromium, molybdenum, zinc, magnesium and copper also were investigated. Matching the calculated and experimental reflectograms leads to the identification of the source of each peak, the establishment of the interband peak energies and the determination of optical constants and thicknesses of the film. The Differential Reflectometer is becoming an important surface analytical instrument comparable with x-ray or Auger analytical techniques.

SECTION I
INTRODUCTION

One of the most serious materials problems today is corrosion. Corrosion costs over eighty billion dollars annually in the United States alone.[1] Corrosion is consuming capital investments including buildings, roads, vehicles and machinery. Costly mineral, energy and human resources are used up to replace the losses. Clearly improvements in corrosion control are of major importance.

To obtain this goal one must have a thorough understanding of corrosion processes. Eight basic forms of corrosion have been identified.[2] Most observed corrosion may be categorized into one or more of these forms. The composition of the corrosion product, its thickness and growth rate are some of the key information needed to understand corrosion mechanisms and facilitate corrosion management.

Corrosion of bulk material commonly involves the formation of a thin film of corrosion product on the outside surface. This thin film is a compound of the base material and some substance(s) from the material environment. For example, Al_2O_3 can form on aluminum exposed to air or oxygen.[3,4] CuO may form on copper and copper alloys exposed to air.

The qualities of the film have a strong influence on the further corrosion behavior of the material.[5] Some films protect the bulk from further corrosion, for example Al_2O_3 protects Al. Other films may not provide protection. The films are initially extremely thin and therefore require special techniques to characterize.

Analysis of the composition and behavior of the thin film is essential in the understanding of the total corrosion response of the material. Knowledge of film composition allows one to observe changes in composition produced by environmental changes and alloying additions. Computation of film growth rates is made possible by film thickness measurements. Thus thin film characterization is a necessary step in understanding corrosion.

A number of techniques are suitable for characterizing thin films. Each has advantages and limitations. There are chemical methods and techniques which probe the electronic structure of the film by sending in energy, particles or electromagnetic waves, and measuring energy absorbed or given off.

Among the most common thin film techniques are Auger Electron Spectroscopy (AES) and Electron Spectroscopy for Chemical Analysis (ESCA). In the case of the AES technique, electrons bombard the sample surface and ejected Auger electrons are detected.[6] In the case of ESCA, x-rays impinge on the sample and ejected electrons are sensed.[7]

Both methods probe the first few atomic layers (about 0.3 nanometers) and are truly surface techniques.

AES and ESCA both suffer from some limitations. Both employ expensive equipment and require skilled operators. But most important, both require that the sample be placed under vacuum. The vacuum may have an effect on the thin, sometimes delicate corrosion films. Both methods are relatively slow, partly due to the vacuum required.

The traditional optical technique for characterizing thin films is ellipsometry. Other optical methods are also in use. They are usually variations of ellipsometry or techniques based on reflection and transmission of light.[8-20] Ellipsometry is the most common method; it measures the extent to which plane polarized incident light is converted to elliptically polarized reflected light. From one set of measurements, two of the three film parameters (n, k, and d) can be calculated if the third is known. The parameter n is the index of refraction, k is the index of absorption and d is the thickness of the film. By performing additional measurements all three parameters may be calculated.[17] In traditional ellipsometry the measurements have to be taken at each desired wavelength. Scanning ellipsometers have overcome this problem.

The new method of Differential Reflectometry (DR)[8] employs a monochromatic beam of light which scans between two samples having slightly different reflectivities (R).

The difference in reflectivity between two samples ($\Delta R = R_1 - R_2$) is electronically divided by the average reflectivity ($\bar{R} = (R_1 + R_2)/2$). The $\Delta R/\bar{R}$ is plotted as a function of wavelength of the light to produce the DR spectrum. This differential reflectogram yields peaks at characteristic energies which can be interpreted by using the electronic band structure of the material under investigation, such as a corrosion film.[8,21,22] Thus Differential Reflectometry provides optical information in a different form than ellipsometry or other transmission and/or reflection techniques.

In previous corrosion studies,[8] DR measurements were made by scanning the light beam between one sample half which consisted of bare metal and the other half which was the same metal covered with a corrosion film. See Figure 1.1. Two types of peaks may appear in the differential reflectograms obtained this way: firstly peaks due to electronic interband transitions and secondly peaks due to interference effects of the thin film on a substrate. In addition to the information obtainable involving only interband peaks, information is also obtainable from the interference peaks. This is possible by using the sample configuration described above in which one sample side is bare metal or by using a configuration in which both sample sides may be oxide covered to different thicknesses. See Figure 1.2. Using the latter technique, n and d may be found for films of

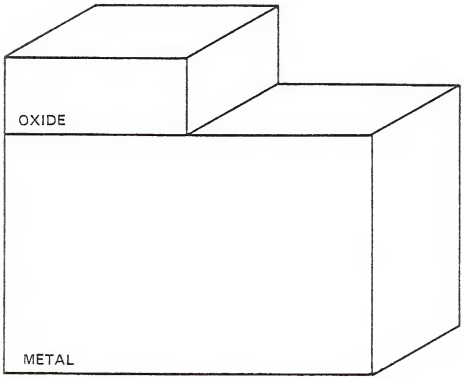

Figure 1.1 Schematic drawing of the sample configuration of a metal oxide on a metal substrate.

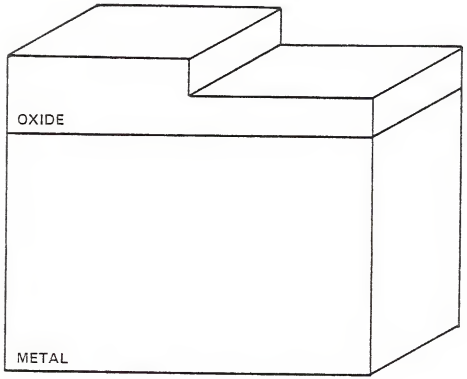

Figure 1.2 Schematic drawing of the sample configuration of metal oxide of two different thicknesses on a metal substrate.

low absorption. In addition the value for k may be obtainable.

The primary advantages of Differential Reflectometry are that measurements can be performed in air as well as in an electrolyte, i. e. in situ, and that extremely small differences in reflectivity may be measured allowing the identification of very thin corrosion films. Measurements are fast; an entire spectrum is recorded within one to three minutes depending upon the scanning speed selected. Finally the measurements cover a continuous band of light wavelengths ranging for example from 200 to 800 nanometers.

In this work a model was developed which takes into account the interactions between the incoming light and an oxide film on a metal substrate. The model relys upon several basic assumptions. Firstly, the validity of the Maxwell equations is assumed. Further the condition that the electric and magnetic fields are continuous at a boundary must hold. Finally it is assumed that no substantial error is introduced by describing the corrosion film as having average optical constants and a uniform thickness even though there may be variations in n and k with depth. From these considerations an equation for the reflectivity may be written that relates the electric field of the incident light to the electric field of the reflected light.

Two reflection equations were written, one for each of the sample halves, see Figure 1.2. The difference of the two calculated reflectivities was divided by their average to obtain $\Delta R/\bar{R}$. The result was plotted as a function of the wavelength of the light. In this way calculated differential reflectograms were generated. The computations were found to be quite elaborate. Therefore, a digital computer was employed to generate the $\Delta R/\bar{R}$ v. s. λ plots.

The normalized differential reflectivities of the corrosion products of various metals were also taken experimentally. The metals which were investigated included copper, magnesium, zinc, molybdenum, chromium and tungsten. The specimens were mechanically polished and heated in dry oxygen to obtain the desired corrosion product. Subsequently part of the corrosion product was removed from one half of the specimen as described in subsection III-4 in order to obtain the step configuration shown in Figures 1.1 and 1.2.

The experimental differential reflectograms were compared with the calculated ones. These studies led to new insights into the general structure of differential reflectograms and how these reflectograms are altered by the thickness of the corrosion films. In section IV the method for determining optical properties and oxide film thicknesses from the experimental curves is discussed.

SECTION II
LITERATURE REVIEW

II-1 Introduction

In the development of a line shape analysis of differential reflectograms of metal-oxide corrosion products, it is necessary to consider previous research in two areas, optical computations and studies of the specific corrosion films in question. The line shape analysis leads to the computation of the optical properties of the corrosion film as well as the identification of the composition of the film. Previous research in optical properties which is relevant to this work includes basic optical theory and various computational techniques. Experimental investigations have been performed on bulk as well as thin film specimens. Previous studies on oxides include thermodynamics, kinetics of formation, crystal structure, transformations, optical and other properties. A review of this work forms a basis for the computer model developed in the next section.

II-2 General Theory of the Optical Properties of Materials

A number of authors have reviewed the theories of the optical properties of materials[23] and the optical properties of metals.[18,24,25] The theories of the

interaction of light with matter form the basis of the methods for calculating the optical parameters n and k. Each of the theories enjoys success within certain ranges of applicability. The Drude free electron theory established in 1899 models a metal as containing a "sea" of free electrons which are able to move in response to an applied electric field. As long as only free electrons are involved, the theory describes observed physical phenomena. Lorenz models insulators as containing bound electrons which are attached to their nuclei by electrostatic forces similar to springs. These electrons are assumed to oscillate in response to an applied ac electric field. The Lorenz model (1910) describes the behavior of insulators although the dc conductivity is not accounted for. A combination of the Drude and Lorenz theories can account for the behavior of most materials over a wide frequency range of the applied electric field.

The quantum-mechanical theory considers electrons to exist in energy bands and to respond to externally applied fields by experiencing interband and intraband transitions. This quantum-mechanical band theory of solids appears to encompass observed light-material interactions.

The values for the index of refraction, n, and the index of absorption, k, are obtainable from the theory in conjunction with experimental measurements. One author[18] notes that although many papers exist in the literature

which deal with optical measurements and computations, there is poor agreement in the values of n and k for the materials studied. Also different values are commonly reported for bulk and for thin film specimens.

In addition to establishing values for n and k, optical property measurements have been shown to provide insight into the electronic band structure of a solid.[8] Reflectivity peaks correspond to interband transition energies and serve as an experimental test of band calculations. With established band diagrams, the peaks may be used to identify an unknown material.

II-3 Techniques for Bulk Optical Properties

Theoretically the interaction of light with a solid is simplest for bulk solids because there are only two media, the specimen and the surrounding medium. Transmission measurements are possible only if the material has a very low absorption constant, i. e. if it is essentially transparent. Reflection measurements on bulk metals have been performed to 0.1% accuracy[26,27] in the ultraviolet, visible and infrared regions of the electromagnetic spectrum. The results are shown to be more accurate when the light impinges upon the material at near-normal incidence.[26]

A number of different approaches have been used to calculate optical properties. A traditional method of

optical measurements is ellipsometry.[28] Ellipsometry measures the extent to which plane polarized light, incident on a material at an angle α is converted upon reflection to elliptically polarized reflected light. The elliptically polarized light may be viewed as a superposition of two normal plane polarized rays with an amplitude ratio Ψ and phase difference Δ. The values of n and k are calculated from Ψ and Δ.

The most popular method in the past twenty years for obtaining the optical properties of metals has been by the measurement of the reflectivity over a large frequency range and obtaining n and k by the Kramers-Kronig analysis. This analysis applies a dispersion relation which relates phase shift at a given frequency to an integral involving the reflectivity at all frequencies.[29,30,31] Unfortunately considerable error may be introduced because the reflectivity is not measured over all frequencies and instead extrapolations must be substituted. Another approach is to use an iterative computer program such as the "NOTS Multilayer Film Program".[10] This program calculates reflection and transmission values from assumed n and k values. The program automatically increments n and k until the resultant calculated reflection and transmission values most closely agree with the experimental values.

Yet another approach is a graphical determination of the optical constants first using light polarized normal

then parallel to the plane of incidence.[32] The value of n and k may be found by varying the angle of incidence, Φ, and plotting the reflection ratio $R_{\parallel}/R_{\perp}$ as a function of Φ, n and k. The surfaces must be very clean for this technique.[33] The measurements are very sensitive to adsorbed species on the surface of the specimen. This effect is the basis for "Surface Reflectance Spectroscopy", a technique which measures adsorbed species on bulk metal.[34]

II-4 Techniques for Absorbing Films

A different approach is required when n and k for thin absorbing films need to be obtained. In a review article, Abelès[35] discusses reflectance, transmittance and ellipsometric techniques which are used to determine n and k for homogenous, isotropic as well as for anisotropic metallic films.

The theory linking these measurements to optical parameters is more complicated than in the bulk case. Equations which relate n and k with reflectivity (R) and transmissivity (T) have been put forth by Heavens.[36] The reflection equation is:

$$R = \frac{(g_1^2+h_1^2)e^{2\alpha_1}+(g_2^2+h_2^2)e^{-2\alpha_1}+A\cos 2\delta_1+B\sin 2\delta_1}{e^{2\alpha_1}+(g_1^2+h_1^2)(g_2^2+h_2^2)e^{-2\alpha_1}+C\cos 2\delta_1+D\sin 2\delta_1} \qquad (2\text{-}1)$$

where

$$A = 2(g_1g_2+h_1h_2) \quad , \tag{2-2}$$

$$B = 2(g_1h_2-g_2h_1) \quad , \tag{2-3}$$

$$C = 2(g_1g_2-h_1h_2) \quad , \tag{2-4}$$

$$D = 2(g_1h_2+g_2h_1) \quad , \tag{2-5}$$

$$g_1 = \frac{n_0^2-n_1^2-k_1^2}{(n_0-n_1)^2+k_1^2} \quad , \tag{2-6}$$

$$g_2 = \frac{n_1^2-n_2^2+k_1^2-k_2^2}{(n_1+n_2)^2+(k_1+k_2)^2} \quad , \tag{2-7}$$

$$h_1 = \frac{2n_0k_1}{(n_0+n_1)^2+k_1^2} \quad , \tag{2-8}$$

$$h_2 = \frac{2(n_1k_2-n_2k_1)}{(n_1+n_2)^2+(k_1+k_2)^2} \quad , \tag{2-9}$$

$$\alpha_1 = \frac{2\pi k_1 d_1}{\lambda} \quad , \tag{2-10}$$

and

$$\gamma_1 = \frac{2\pi n_1 d_1}{\lambda} \quad . \tag{2-11}$$

The transmission equation is:

$$T = \frac{n_2}{n_0} \frac{((1+g_1)^2+h_1^2)((1+g_2)^2+h_2^2)}{e^{2\alpha_1}+(g_1^2+h_1^2)(g_2^2+h_2^2)e^{-2\alpha_1}+C\cos 2\gamma_1+D\sin 2\gamma_1} \qquad (2\text{-}12)$$

These equations apply to a thin absorbing film on an absorbing substrate. The indices of refraction are as follows:

n_0 = index of refraction of surrounding, non-absorbing medium

n_1 = index of refraction of the absorbing film

k_1 = index of absorption of absorbing film

n_2 = index of refraction of absorbing substrate

k_2 = index of absorption of absorbing substrate .

The complex index of the film is

$$\hat{n}_1 = n_1 - ik_1 \quad , \qquad (2\text{-}13)$$

and that of the substrate is

$$\hat{n}_2 = n_2 - ik_2 \quad . \qquad (2\text{-}14)$$

These equations may be simplified, with some loss in accuracy. The approximations may be solved graphically or numerically for n and k of the films.[19] The graphical technique using the reflection ratio, $\Delta R / \bar{R}$, mentioned in subsection II-3 is also possible for thin films.[16]

The application of digital computers to calculate n and k has allowed more accurate and faster methods. An iterative "hill-climbing" technique was described by Ward et al.[37] utilizing data from reflection and transmission measurements using incident light of parallel and normal polarization. To accomplish this an objective function, y, is formed:

$$y = (R_p(\text{expt.})-R_p(n,k,d))^2 + (R_s(\text{expt.})-R_s(n,k,d))^2$$

$$+(T_p(\text{expt})-T_p(n,k,d))^2+(T_s(\text{expt.})-T_s(n,k,d))^2 \quad (2\text{-}15)$$

where

$R_p(\text{expt.})$ = experimentally measured reflection of parallel polarized incident light,

$T_s(n,k,d)$ = calculated value of transmission of normally polarized incident light.

The values of n, k and d are varied until y in equation (2-15) reaches a preselected small value. The associated values of n, k and d are then taken to be those of the film.

The Heavens equations may be directly used to obtain computer calculated solutions for the optical constants through another method. Reflection and transmission measurements at near-normal incidence allow the calculation of the optical constants as long as an independent measure of the thickness is known.[17,38-41] The computer methods are in general iterative, solving for the values of n and k which produce a close match between the measured and calculated values of reflection and transmission.

The optical constants of a thin film deposited on a non-absorbing substrate may be calculated from transmittance using a Kramers-Kronig analysis.[42] The equations relate the real and imaginary parts of the transmittance. The real part is the change in amplitude and the imaginary part is the change in phase of the light.

II-5 Techniques for Non-absorbing Films

Techniques have been developed for non-absorbing thin films on absorbing substrates. These are reviewed by Bennett and Bennett.[9] Methods for calculating optical properties and thickness of non-absorbing thin films using ellipsometry have been reviewed by Neal and Fane.[28] In the case of thin films, the same type of measurements are performed as for bulk materials.[43,44] Two of the values of n, k and d may be calculated from a single ellipsometric

measurement. All three parameters may be found from two ellipsometric measurements at differing angles of incidence. It is possible to calculate the refractive index, n, and thickness, d, from one ellipsometric measurement taken at a single angle of incidence by neglecting the absorption, k. The error in the calculated n and d has been shown to be more significant for low index films.[45]

Each ellipsometric measurement is taken at a particular light wavelength. Thus, many measurements must be made to obtain the spectral dependence of the optical properties.

Differential Reflectometry has been shown to correlate signal intensity to thickness for low absorbing films on metal substrates.[8,21]

II-6 Non-uniform Films

All the methods previously discussed assume homogeneous, isotropic films which are perfectly flat and are deposited on a flat substrate. The problems introduced by the conditions of non-uniformity, anisotropy, inhomogeneity and surface roughness have been the subject of inquiry by a number of investigators. An early study explains how the apparent color of a glass can be produced by the presence of microscopic particles of metal.[46] It has been shown[47] that average values of the optical properties can be used instead of a continuous variation in optical properties.

It also has been shown that it is possible to represent a real surface film having a rough surface with an equivalent flat film having a perfectly smooth surface.[48] The notion of an equivalent flat film is further supported by results originating from ellipsometric measurements on absorbing films in which the calculated film thickness was in agreement with two independent thickness measuring techniques.[49] This result is particularly important for the development of the model in the following section.

Polishing techniques affect the surface roughness and hence the measured reflectance.[50] This fact throws all absolute measurements into question since none of the authors reported or controlled surface roughness. The Differential Reflectometry technique circumvents this problem by comparing two surfaces which are equally prepared and hence surface roughness effects are subtracted out instrumentally.

A method for ellipsometric measurements and calculations for films containing foreign particles has been developed.[51] The foreign material was treated as though it were an equivalent film, in addition to the film in which the particles are located. The equivalent film was assumed to have the same volume as the total volume of the foreign particles.

Computations for multilayer thin films have also been investigated. Weinstein[52] discusses various approaches

to computing thin film optical constants with particular attention to multilayer films. He describes graphical and explicit formula methods for obtaining reflection magnitude by keeping track of the E and H fields of the incident and subsequently multiply reflected and transmitted electromagnetic waves. The transmission and reflection factors are found by assuming continuity of the E and H fields at a boundary. He concludes that for the purpose of multilayer film design, the four terminal network model is insufficient in that it cannot account for the polarization and obliqueness of incidence.

II-7 Metal Oxides

The oxidation of metals is by no means an untouched field. A complete review of the literature is beyond the scope of this work. An excellent early review is given by McAdam and Geil.[53] There are a number of texts in the field including one by Fromhold.[54] The following focuses upon three specific areas involving metal oxides. These are optical properties, phase diagrams and electronic structure of the metal oxides of particular interest. Since the primary thrust of this work is in the tungsten-oxygen system, most of the previous work in this area is shown here. Other metal-oxygen systems were investigated primarily to support the findings for tungsten oxide.

II-8 Optical Properties

The optical properties of two tungsten oxides, WO_2 and WO_3, have been reported by several authors. Dissanayake and Chase[55] recorded the reflectivity of WO_2 as a function of energy. By using the Kramers-Kronig analysis described in subsection II-3, the real and imaginary parts of the dielectric constant, $\hat{\varepsilon}$, of WO_2 were found, Figure 2.1. In Figure 2.2 the spectral reflectivities of WO_2 and MoO_2 are shown. The following equations relate the optical constants to the dielectric constants:

$$\hat{\varepsilon} = \hat{n}^2 = (n - ik) \quad , \tag{2-16}$$

where

$$\varepsilon_1 = n^2 - k^2 \tag{2-17}$$

and

$$\varepsilon_2 = 2nk \tag{2-18}$$

where

$$\hat{\varepsilon} = \varepsilon_1 + i\varepsilon_2 \quad . \tag{2-19}$$

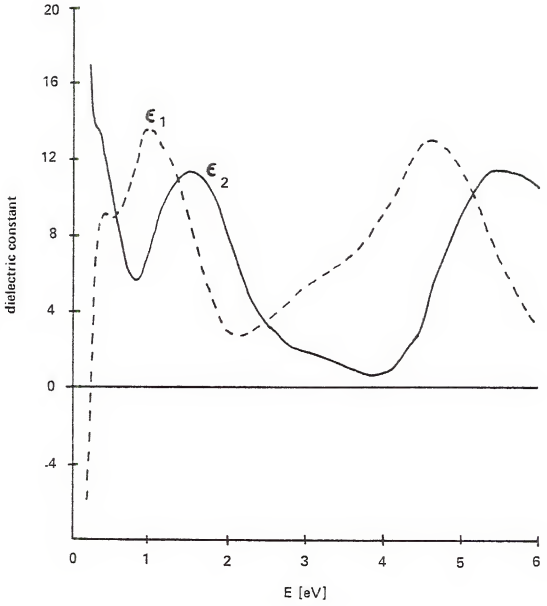

Figure 2.1 Real (ϵ_1) and imaginary (ϵ_2) parts of the dielectric constant of WO_2. (reference 55)

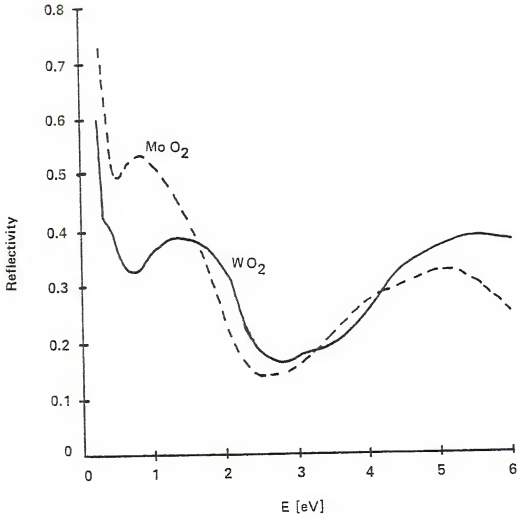

Figure 2.2 Unpolarized reflectivity spectra of WO_2 and MoO_2 at 300 ^{o}K. (reference 55)

The index of refraction of WO_3 was reported by Sawada and Danielson[56] to be n = 2.45. They measured an average value over crystallographic direction using white light from a tungsten source. Deb reported[57] the spectral dependence of n for WO_3 from 450 to 1799 nanometers, Figure 2.3. The average value reported by Deb is in good agreement with the value obtained by Sawada and Danielson. Deb also reported optical absorption, k, of WO_3 as shown in Figure 2.4 He reports absorption peaks at 4.39 eV (282 nm) and at 5.25 eV (236 nm) for thin films. These peaks moved to lower energies (longer wavelengths) with increased annealing time. Deb observed that the thin films are commonly amorphous and suggests that this fact may explain the lack of certain absorption peaks predicted by band calculations based upon the assumption of crystalline material. He reported an absorption peak for MoO_3 at 2.85 eV (434 nm) for thin films.[58,59] The index of refraction of MoO_3 is shown in Figure 2.5 as measured by Deb. Chase[60] has determined the dielectric constants of CrO_2 and MoO_2 and these are presented in Figure 2.6 and Figure 2.7.

Ellipsometric and transmission investigations of the optical properties of ZnO show an interband feature at 3.3 eV (375 nm). In an investigation using ellipsometric spectroscopy on the ZnO nonpolar (1100) surface, Matz and Luth[61] report the values of n and k of bulk ZnO. See Figure 2.8 and Figure 2.9 Aranovich et al.[62] report the

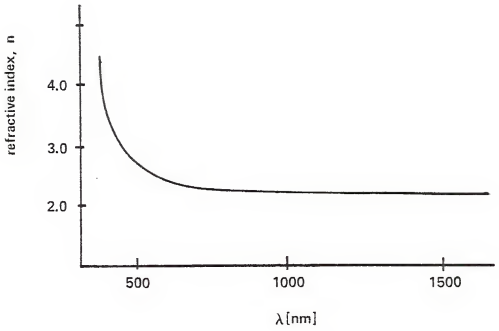

Figure 2.3 The refractive index, n, of amorphous WO_3 films as a function of light wavelength. (reference 57)

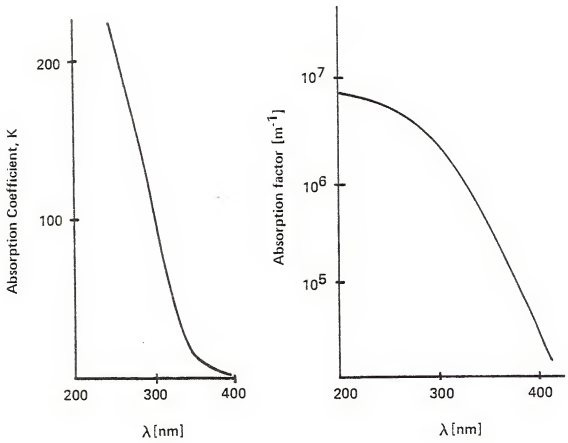

Figure 2.4 The absorption factor of amorphous WO_3 films is reported in the right graph of the figure. The data is replotted in the left graph to conform to the definition of the absorption coefficient, k, where absorption factor = $4\pi k/\lambda$. (reference 57)

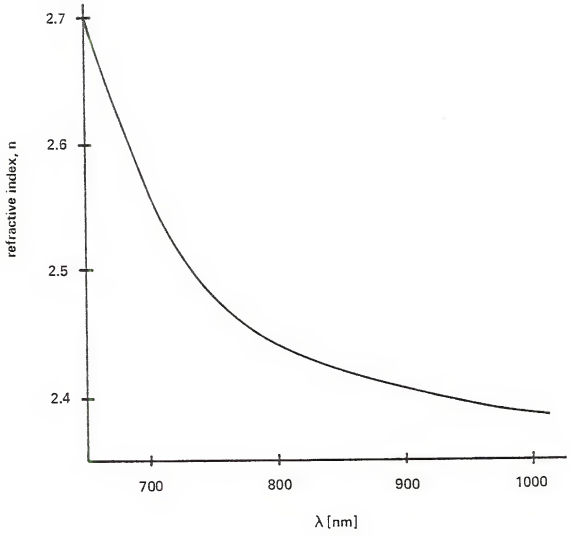

Figure 2.5 The refractive index, n, of MoO_3 thin films as a function of wavelength. (reference 58)

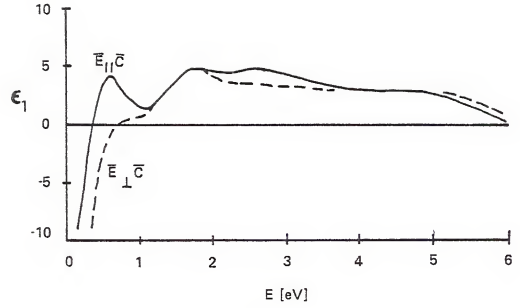

Figure 2.6 Real part of the dielectric constant ϵ_1 of CrO_2 as a function of photon energy. (reference 60)

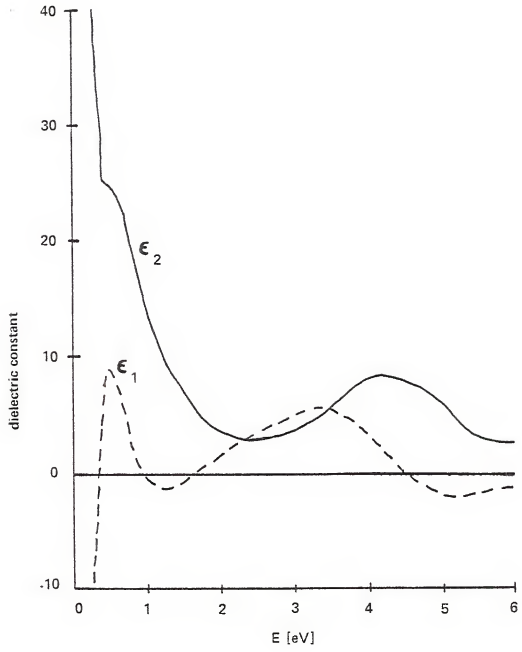

Figure 2.7 Dielectric constant of MoO_2 as a function of photon energy. (reference 60)

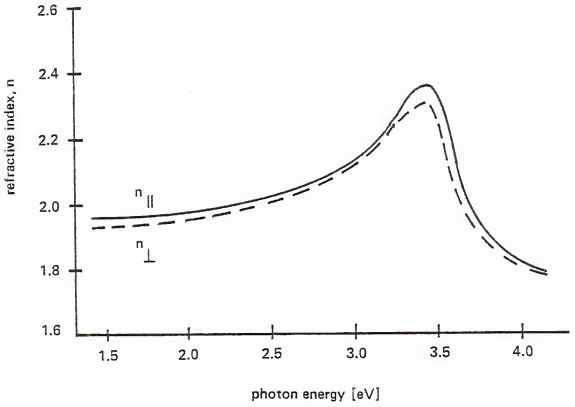

Figure 2.8 Optical index of refraction of ZnO at room temperature as measured by ellipsometry. (reference 61)

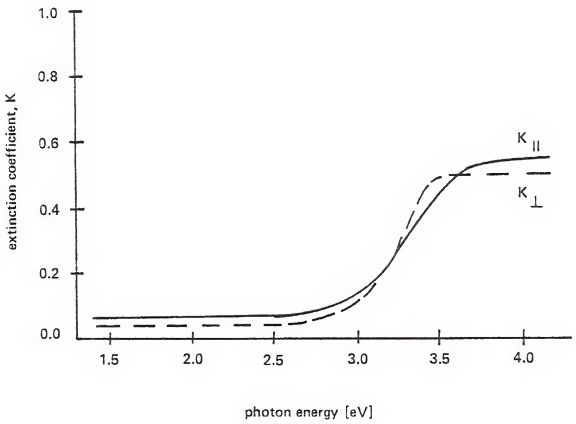

Figure 2.9 Optical extinction coefficient, k, of ZnO at room temperature as measured by ellipsometry. (reference 61)

transmission of ZnO as a function of wavelength from 300 to 900 nanometers, see Figure 2.10.

The reflectivity of Cu_2O is reported by Brahms and Nikitine[63] as shown in Figure 2.11. The electroreflectance of Cu_2O is reported by Daunois et al.[64] as shown in Figure 2.12. Ladelfe et al.[65] present the optical constants of Cu_2O. These are shown in Table 2.1.

II-9 Phase Diagrams

A number of phase diagrams of the tungsten-oxygen system have been published.[66-68] The phase diagram of St. Pierre et al.[68] is presented in Figure 2.13. It can be seen that below 484 °C the only phases thermodynamically expected are W_3O, WO_2 and WO_3. Between 484 °C and 585 °C $W_{20}O_{58}$ becomes thermodynamically stable. Above 585 °C $W_{18}O_{49}$ also becomes stable.

II-10 Electronic Structure

The electronic structures of cubic $NaWO_3$ and of $NaWO_3$ with a vacancy on the Na site have been calculated. Figure 2.14 presents the band diagram of $\square WO_3$.[69] It can be seen that four symmetry point interband electron transitions are indicated. The Γ point transition is generally believed not to occur. It has the same energy as the X point transition, 1.9 eV (651 nm). The M point transition is at 4.6 eV (269 nm) and the R point transition is at 6.12 eV (202 nm).

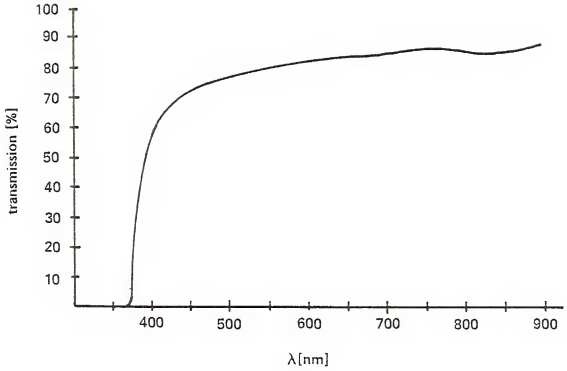

Figure 2.10 Optical transmission of a ZnO film.
(reference 62)

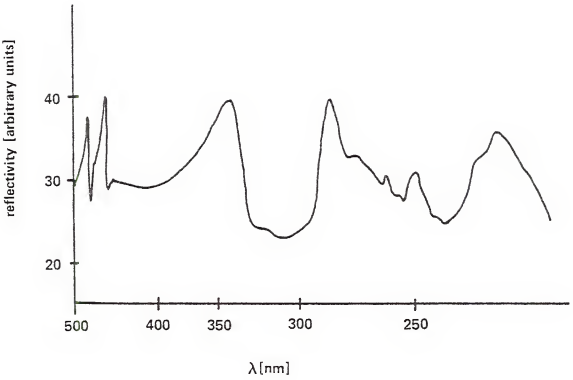

Figure 2.11 Reflectivity of cuprous oxide (Cu_2O) single crystal at 77 ^{o}K. (reference 64)

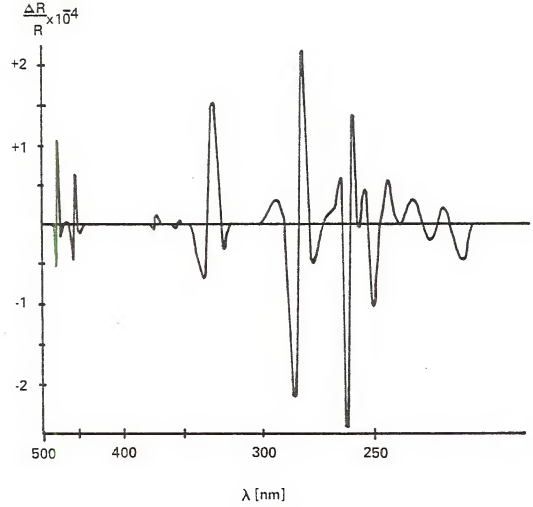

Figure 2.12 Electroreflectance of Cu_2O at 85 °K in a field, E = 60 kV/cm. (reference 64)

TABLE 2.1

The wavelength dependence of n and k for CuO films.

wavelength (nm)	n	k
450	2.45±0.08	0.744±0.011
500	2.59±0.09	0.650±0.017
550	2.57±0.10	0.539±0.019
600	2.60±0.11	0.449±0.025
650	2.65±0.12	0.345±0.028
700	2.64±0.13	0.236±0.030
750	2.65±0.10	0.170±0.024
800	2.62±0.09	0.123±0.022

(reference 65)

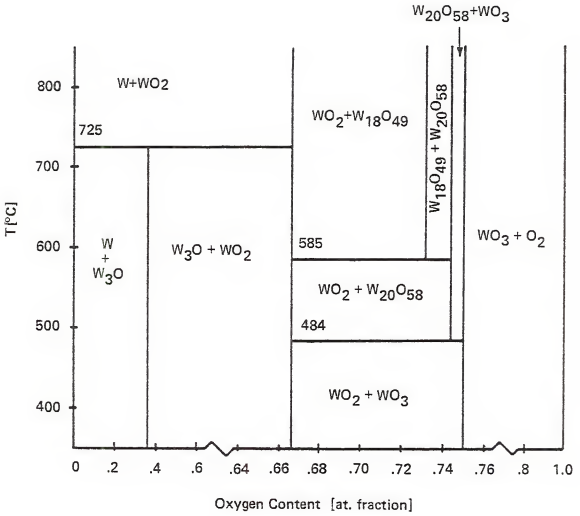

Figure 2.13 Phase diagram of tungsten-oxygen at atmospheric pressure. (reference 68)

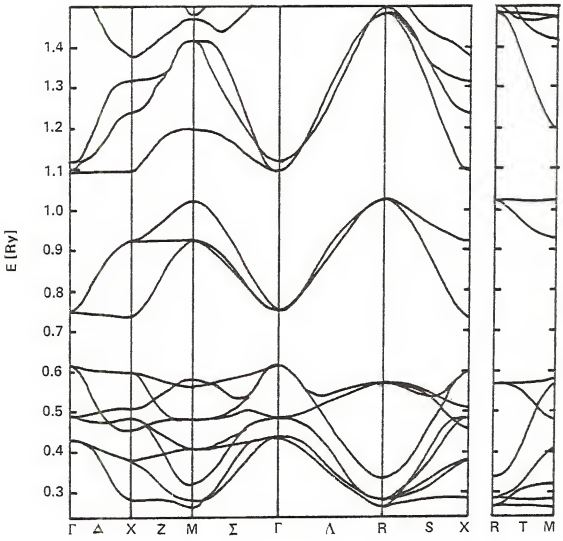

Figure 2.14 Energy bands of $NaWO_3$ with a vacancy on the Na site along the symmetry axes.

SECTION III
EXPERIMENTAL PROCEDURE

III-1 Introduction

The basic steps of the experimental procedure are sample preparation, corrosion, preparation for measurement and recording the differential reflectogram.

III-2 Sample Preparation

Discs, approximately 25 mm in diameter and 12 mm high were cut from high purity rods. Table 3.1 lists the sources and purities. One part of the disc was cut away to produce a "D" shaped sample, Figure 3.1. The flat side of the sample serves as a guide for the half polishing technique (see below).

Rough polishing was performed using 180, 320 and finally 600 grit silicon carbide paper using soap as a lubricant, followed by Microcut Paper Sheets* to remove the silicon carbide grit from the sample. The samples were then polished on polishing cloth to a 6μ diamond and finally to a 1μ diamond finish using Metadi Fluid** as a lubricant. This procedure worked well for most metals.

---

*Microcut (registered) Paper Sheets, Buehler Ltd., Evanston, Illinois

** Metadi Fluid (registered), Buehler Ltd., Evanston Illinois

TABLE 3.1

Sources of metals.

metal	source
tungsten	A. D. MacKay, Rare Metals and Chemicals, 10 Center St. Daren, CT 06820
molybdenum	same
magnesium	same
zinc	same
copper	same
chromium	Materials Research Corp., Orangeburg, New York 10962

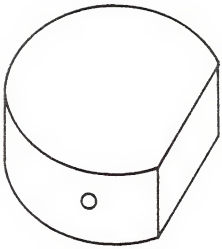

Figure 3.1 Sample configuration for corrosion experiments. The hole is to allow a thermocouple to be inserted into the sample.

In the case of zinc however, Emery Paper Sheets* , grades 1 through 0000, were used. The papers were lubricated by rubbing them with wax and applying a light coating of mineral spirits. The samples were rinsed in mineral spirits before changing to a finer grade of paper. Samples were rotated 90° between each grade.

After polishing, the specimens were rinsed with a soap-water mixture, followed by a rinse in methanol and drying in a stream of filtered air. Finally the samples were warmed by hot air to reduce the possibility of water condensation on the surface.

It was observed that one of the corrosion products of molybdenum dissolved in water. Therefore these samples were rinsed in methanol only.

III-3 Corrosion

The metal discs were positioned in a quartz tube and heated in a radiant furnace, Figure 3.2. During heating, dried** oxygen is passed over the specimens. The temperature of the sample was measured using a thermocouple inserted into a hole in the metal disc.

Specimen temperature was controlled by a variable transformer. Figure 3.3 shows a typical temperature curve.

---

*Emery Paper Sheets, Buehler Ltd., Evanston, Illinois

**W. A. Hammond Drierite Co., Xenia, Ohio

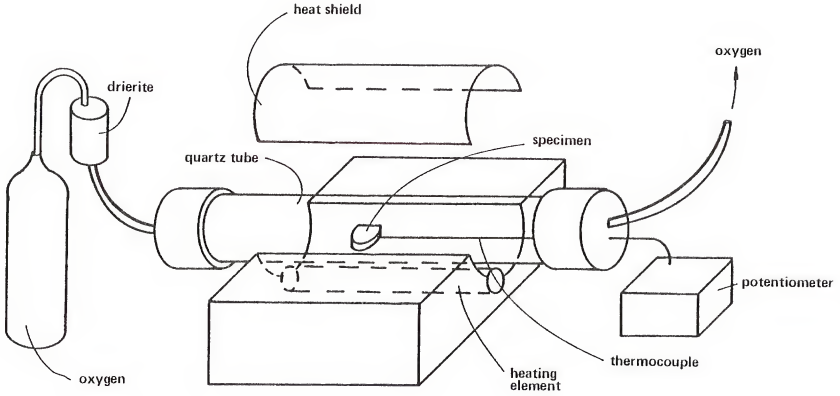

Figure 3.2 Schematic drawing of the corrosion furnace. Dried oxygen enters at the left. The specimen is heated by radiant heat.

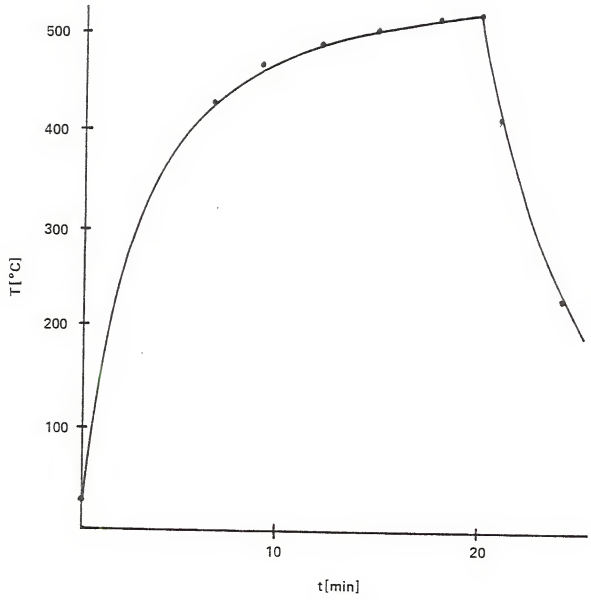

Figure 3.3 Temperature of a tungsten disc as a function of time as measured by a thermocouple mounted inside the disc. Power was applied at zero time and removed at twenty minutes.

Most specimens were heated for twenty minutes. Heating less than twenty minutes resulted in temperatures which did not approach a constant level, Figure 3.3. At longer heating times the corrosion product became too thick and opaque for useful optical measurements. At the end of each heating the sample was allowed to cool in an oxygen atmosphere.

III-4 Half-polishing

Corrosion product on half of the specimen was polished partly or completely away using a polishing gauge, polishing cloth, 1μ diamond polishing compound* and Metadi Fluid** as a lubricant. Figure 3.4 shows how the flat side of the sample serves as a guide. To remove a small amount of corrosion product, very light pressure was applied and the sample was moved only a few cm along the guide. As before the sample was rinsed with alcohol, dried with dessicated air and gently warmed with hot air. After this procedure the sample had the configuration of Figure 1.1 or 1.2. The sample was then immediately transferred into the instrument and a differential reflectogram was taken. Since any further oxidation caused by the environment is believed to affect both

*Metadi Diamond Polishing Compound (registered), Buehler Ltd., Evanston, Illinois

**Metadi Fluid (registered), Buehler Ltd., Evanston Illinois

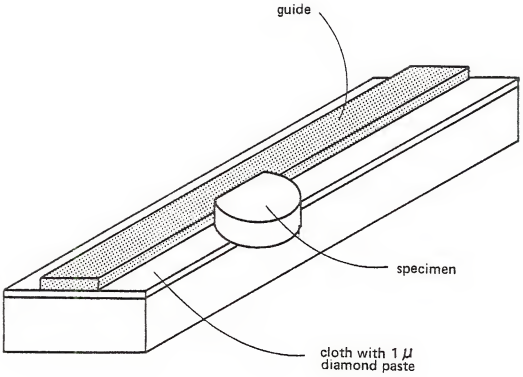

Figure 3.4 This schematic drawing of the half-polishing guide shows how the sample may be accurately positioned to remove corrosion product from part of the reacted surface.

sides of the sample equally, the formation of further corrosion products can essentially be neglected.

III-5 The Differential Reflectometer

The Differential Reflectometer has been described in detail elsewhere.[8,21] Thus only a brief description of the instrument and its operation is given here.

Absolute reflectivity measurements are extremely difficult to make with a high degree of accuracy except for vapor deposited films in high vacuum. Surface contamination, surface preparation, variation in light source output, line voltage changes and sample alignment all contribute to error. The problems are exaggerated when an attempt is made to measure a small reflectivity difference between slightly different alloys or metals covered with thin films. A differential technique has been developed especially to make these kinds of measurements. The Differential Reflectometer is capable of detecting differences in reflectivity as small as 0.001%.

Briefly the DR technique produces a plot of the difference in reflectivity between two sample areas, divided by the average reflectivity, versus light wavelength. A high pressure xenon light source provides a broad band output to the scanning monochromator, Figure 3.5. The very narrow bandwidth light beam emerging from the monochromator is focused by mirrors onto an

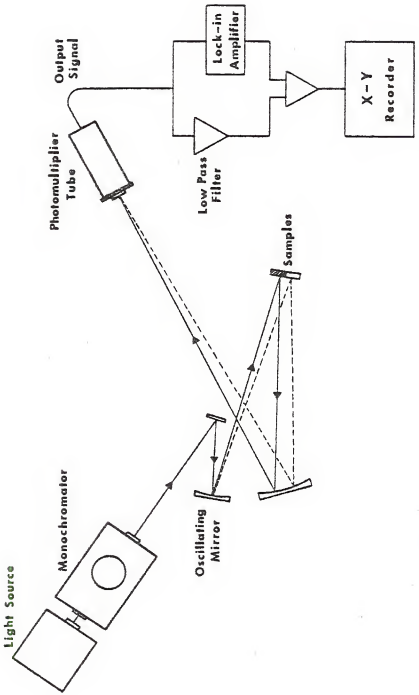

Figure 3.5 Schematic drawing of the differential reflectometer.

approximately 2 mm diameter spot on the sample. One of the mirrors vibrates at 60 Hz and scans the spot up and down about 6 mm. The scan dimensions are adjustable by regulating the voltage to the coil of the vibrating mirror.

The operator can manually shift the sample position to cause the beam to spend half of the scan time on each part of the sample. An oscilloscope trace is used to monitor the reflected intensities of each specimen half, thus allowing very accurate positioning of the sample. The reflected beam is directed onto a frosted quartz glass plate immediately in front of the photomultiplier tube to diffuse the beam evenly over the photosensitive surface.

The photomultiplier output consists of a direct current component modulated by a 60 Hz square wave whose amplitude is proportional to ΔR. By means of a lock-in amplifier tuned to 60 Hz, the square wave is detected and a direct current signal proportional to the difference in reflectivity (ΔR) is produced. A low pass filter smooths the 60 Hz square wave modulation in the original signal to produce a signal proportional to the average reflectivity ($\bar{R}$). These two signals are passed to a divider where the ratio, $\Delta R/\bar{R}$, is formed.

The monochromator produces a direct current voltage proportional to wavelength. This signal is applied to

the X axis of the X-Y recorder. The $\Delta R/\bar{R}$ signal is applied to the Y axis. A DR spectrum is obtained by scanning the wavelengths from 200 to 800 nanometers. A typical scan takes approximately one and one-half minutes.

III-6 Summary

Samples were prepared from high purity metals. The samples were polished on one surface to an optical quality, 1μ diamond finish.

Each sample was individually heated in a furnace in a dried oxygen atmosphere. The corroded sample was half-polished to produce a step in the corrosion product film and the differential reflectivity between the corroded and polished areas was recorded as a function of wavelength.

SECTION IV
RESULTS AND DISCUSSION

IV-1 Introduction

This section presents model calculations for the normalized difference in reflectivity ($\Delta R/\bar{R}$) versus light wavelength λ for a metal/metal-oxide couple as would be expected by measurements using a differential reflectometer. Much information exists in these reflectograms. A set of equations or an algorithm was developed to extract certain data from the experimental curves. From these the index of refraction, n, the index of absorption, k, and the thickness, d, of the oxide film may be calculated. In other words a bridge between the DR spectrum and n, k and d of the film was developed.

IV-2 Model Geometry

For the model used here, an average complex index of refraction, $\hat{n}$, is assumed for each medium. This complex index of refraction contains the real index of refraction, n, and the real index of absorption, k:

$$\hat{n} = n - ik \qquad (4\text{-}1)$$

In Figure 4.1 let medium "0" be air or an electrolyte,

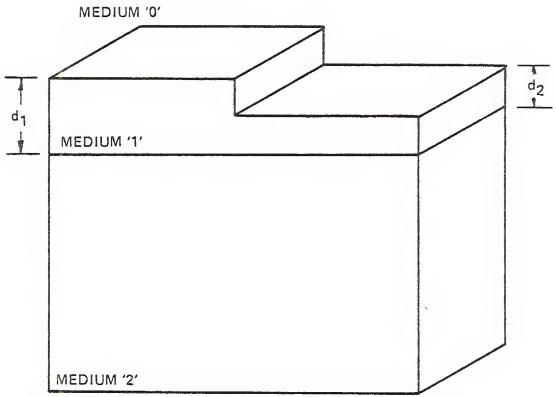

Figure 4.1 Geometric configuration of the model used in this work.

medium "1" be the oxide and medium "2" be the metal substrate. The light beam of the differential reflectometer is thought to scan between the two parts of this sample and thus produce the $\Delta R/\bar{R}$ curve as described in section III.

IV-3 Interaction Between Light and Matter

A light ray which impinges upon a sample from medium "0" (r_0) is partly reflected (r_1) and partly transmitted (r_2) into medium "1", Figure 4.2. The transmitted wave (r_2) is attenuated as it passes through medium "1" having a thickness, d. This attenuated wave is partly reflected (r_4) and partly transmitted into medium "2" (r_3). Ray (r_4) is again attenuated by medium "1". Finally this wave reaches the 0-1 interface and is partly reflected (r_6) and partially transmitted (r_5). Rays r_1 and r_5 are assumed to add by superposition. The internal reflection process in medium "1" continues with ever diminishing contributions from each subsequent reflection. Appendix B shows how these considerations may be taken into account. In this work however, the additional contributions are considered to be negligibly small and are therefore omitted.

The Maxwell equations,

$$\text{curl } \hat{\underline{H}} = \dot{\hat{\underline{E}}}\,\varepsilon/c + \hat{\underline{E}}\,4\pi\sigma/c \quad , \tag{4-2}$$

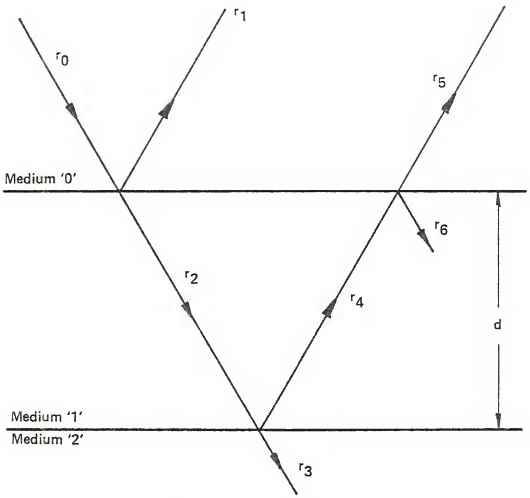

Figure 4.2 Interactions between a light beam, r_0, and a solid consisting of a semi-transparent medium "1" (e. g. oxide film) and an absorbing medium "2" (e. g. metal). For clarity the incident, reflected and transmitted rays are shown at an angle. The calculation is carried out assuming normal incidence.

and

$$\text{curl } \hat{\underline{E}} = -\dot{\hat{\underline{H}}}\mu/c \quad , \tag{4-3}$$

can be solved by assuming a plane polarized wave propogating in the z direction having an electric field strength E_x given by

$$\hat{E}_x = E_0 \, e^{i\omega(t - \hat{n}z/c)} \quad , \tag{4-4}$$

where

$\hat{E}_x$ = complex value of the magnitude and phase of the x component of the electric field,

E_0 = the real value of the peak of the electric field,

e = the natural base,

i = the square root of -1,

ω = the radian frequency of the electromagnetic wave,

t = time,

$\hat{n}$ = complex index of the medium in which the wave propagates,

z = z axis position, axis of propogation,

c = speed of light,

$\hat{\varepsilon}$ = permittivity of the medium,

σ = conductivity of the medium,

$\hat{\underline{H}}$ = magnetic field vector,

μ = permeability of the medium and

$\hat{\underline{E}}$ = the electric field vector.

The electric field strengths of the incident, reflected and transmitted waves at a given boundary are related by the materials properties. The following equations hold, see figure 4.3.

$$\hat{T}_{ab} = \hat{E}_t/\hat{E}_i = 2\,\hat{Z}_b/(\hat{Z}_b + \hat{Z}_a) \qquad (4\text{-}5)$$

and

$$\hat{P}_{ab} = \hat{E}_r/\hat{E}_i = (\hat{Z}_b - \hat{Z}_a)/(\hat{Z}_b + \hat{Z}_a) \quad . \qquad (4\text{-}6)$$

They are derived in Appendix A. In these equations

$\hat{T}_{ab}$ = the ratio of the transmitted electric field strength in medium "b" to the incident field in "a" ,

$\hat{P}_{ab}$ = ratio of the reflected electric field in medium "a" to the incident field in "a", reflection occurs at the a-b interface,

$\hat{E}_i$ = the complex electric field strength of the incident electromagnetic wave,

$\hat{E}_t$ = the complex electric field strength of the transmitted electromagnetic wave,

$\hat{E}_r$ = the complex electric field strength of the reflected electromagnetic wave,

$\hat{Z}_a$ = the complex impedance of medium "a" (note that by definition impedance is the ratio of the x component of the E field to the y component of the H field in medium "a". These vectors are normal to each other and to the direction of propagation. The material may be anisotropic)

$\hat{Z}_b$ = the complex impedance of medium "b" .

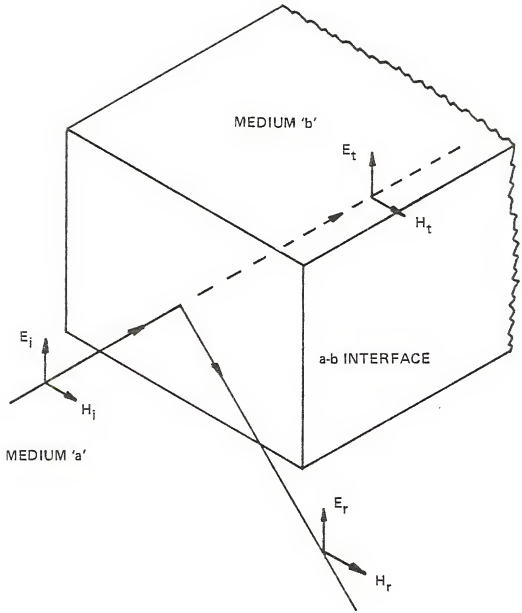

Figure 4.3 Reference directions for the incident, transmitted and reflected E and H components of an electromagnetic wave. The rays are shown at an angle for clarity only.

Equations (4-5) and (4-6) result from assuming continuity of E and H fields at an interface. The notation of media "a" and "b" has been chosen in order to emphasize the general nature of the equations.

It is possible to express $\hat{Z}$ in terms of $\hat{n}$ in order to rewrite equations (4-5) and (4-6) in terms of the variables of the model, $\hat{n}_0$, $\hat{n}_1$ and $\hat{n}_2$. See the derivation in Appendix A, subsection A-2. Thus we write

$$\hat{Z} = \mu / \hat{n} \quad . \tag{4-7}$$

In the following, magnetic influences are not considered. Therefore μ is set to unity. This yields for medium "a" and medium "b",

$$\hat{Z}_a = 1 / \hat{n}_a \tag{4-8}$$

and

$$\hat{Z}_b = 1 / \hat{n}_b \quad . \tag{4-9}$$

Substituting (4-8) and (4-9) into (4-5) and (4-6) yields

$$\hat{T}_{ab} = 2 \hat{n}_b / (\hat{n}_a + \hat{n}_b) \tag{4-10}$$

and

$$\hat{P}_{ab} = (\hat{n}_a - \hat{n}_b) / (\hat{n}_a + \hat{n}_b) \quad . \tag{4-11}$$

Now it is possible to write the specific transmission and reflection ratios which appear in the model at the 0-1 and 1-2 interfaces. Figure 4.3 defines the incident field direction relative to the locations of the two media composing the interface. The reflection ratio for an incident field in medium "0" falling on an interface with medium "1" is

$$\hat{P}_{01} = (\hat{n}_0 - \hat{n}_1) / (\hat{n}_0 + \hat{n}_1) \quad . \tag{4-12}$$

The transmission ratio for an incident field in medium "0" passing into medium "1" is

$$\hat{T}_{01} = 2\,\hat{n}_1 / (\hat{n}_0 + \hat{n}_1) \quad . \tag{4-13}$$

The reflection ratio for an incident field in medium "1" reflecting from an interface with medium "2" is

$$\hat{P}_{12} = (\hat{n}_1 - \hat{n}_2) / (\hat{n}_1 + \hat{n}_2) \quad . \tag{4-14}$$

The transmission ratio for an incident field in medium "1" passing into medium "0" is

$$\hat{T}_{10} = 2\,\hat{n}_0 / (\hat{n}_1 + \hat{n}_0) \quad . \tag{4-15}$$

The equation for the attenuation of the electric field as the wave penetrates perpendicularly into a medium can be written according to (4-4). See Appendix A, subsection A-3.

$$\hat{A} = e^{-i\omega \hat{n} d/c} \quad . \tag{4-16}$$

Applying this to thicknesses d_1 and d_2 of Figure 4.1 yields

$$\hat{A}_{d1} = e^{i\omega \hat{n}_1 d_1/c} \tag{4-17}$$

and

$$\hat{A}_{d2} = e^{i\omega \hat{n}_1 d_2/c} \quad . \tag{4-18}$$

It is now possible to write an equation in accordance with the reflection model of Figure 4.4. Let the incident plane wave contain the electric field, $\hat{E}_i$. Consider the series of interactions in Figure 4.4.

$$\hat{E}_{d1} = \hat{E}_i \left(\hat{P}_{01} + \hat{T}_{01} \hat{A}_{d1} \hat{P}_{12} \hat{A}_{d1} \hat{T}_{10} \right) \quad . \tag{4-19}$$

Similarly for thickness d_2

$$\hat{E}_{d2} = \hat{E}_i \left(\hat{P}_{01} + \hat{T}_{01} \hat{A}_{d2} \hat{P}_{12} \hat{A}_{d1} \hat{T}_{10} \right) \quad . \tag{4-20}$$

Because the photomultiplier is sensitive to intensity i. e. to $|E|^2$ we obtain

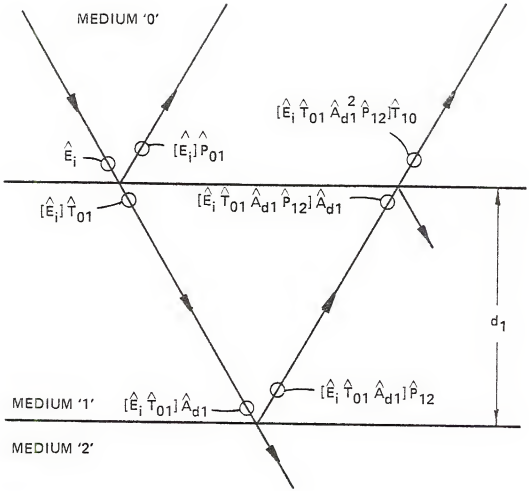

Figure 4.4 Schematic representation of the reflection of an electromagnetic wave from a thin film covering a substrate. The incident wave begins at the upper left. At each significant point along the way, the E field is indicated. For clarity the incident, reflected and transmitted rays are shown at an angle. The calculations are carried out assuming normal incidence.

$$\Delta R/\bar{R} = 2\,(|\hat{E}_{d1}|^2 - |\hat{E}_{d2}|^2)/(|\hat{E}_{d1}|^2 + |\hat{E}_{d2}|^2). \quad (4\text{-}21)$$

Combining (4-19) through (4-21) yields

$$\frac{\Delta R}{\bar{R}} = 2\,\frac{|\hat{P}_{01}+\hat{T}_{01}\hat{A}_{d1}^2\hat{P}_{12}\hat{T}_{10}|^2 - |\hat{P}_{01}+\hat{T}_{01}\hat{A}_{d2}^2\hat{P}_{12}\hat{T}_{10}|^2}{|\hat{P}_{01}+\hat{T}_{01}\hat{A}_{d1}^2\hat{P}_{12}\hat{T}_{10}|^2 + |\hat{P}_{01}+\hat{T}_{01}\hat{A}_{d2}^2\hat{P}_{12}\hat{T}_{10}|^2} \quad (4\text{-}22)$$

Equation (4-22) expresses the normalized difference in reflectivity in terms of the physical parameters of the model, $\hat{n}_0$, $\hat{n}_1$, $\hat{n}_2$, d_1 and d_2 which are contained in the $\hat{A}$'s, $\hat{T}$'s and $\hat{P}$'s.

IV-4 Computer Program

In order to obtain a differential reflectogram from equation (4-22) it is necessary to plot the value of $\Delta R/\bar{R}$ as a function of wavelength λ. Recall that for light waves

$$c = \lambda\nu = \lambda\omega/2\pi$$

or

$$\omega = 2\pi c/\lambda \quad (4\text{-}23)$$

The value of λ appears in $\hat{A}_{d1}$ and $\hat{A}_{d2}$ of equations (4-17) and (4-18). The values of $\hat{P}_{01}$, $\hat{T}_{01}$, $\hat{P}_{12}$ and $\hat{T}_{10}$ will also be functions of wavelength if the values of $\hat{n}_0$, $\hat{n}_1$ and $\hat{n}_2$ are functions of wavelength. Because the n's are

not all known in advance, a difference approach is used in which the values of the unknown $\hat{n}$'s are assumed to be constant with wavelength. As solutions are achieved, the unknown dependence may be found by interpreting the difference in the calculated and the experimental reflectogram to be due to the variation of $\hat{n}$ with wavelength.

Literature studies have shown that in a number of instances the complex index of refraction for a metal is nearly constant with wavelength over the range from 200 to 800 angstroms. In the case of air, $\hat{n}_0 = 1 + i0$; therefore $\hat{n}_0$ is constant with wavelength.

A digital computer was used to calculate and plot theoretical reflectograms ($\Delta R/\bar{R}$ versus λ) using equations (4-12), (4-13), (4-14), (4-15), (4-17), (4-18) and (4-22). The program is listed in Appendix D. The computer was programmed to calculate $\Delta R/\bar{R}$ for 800 individual wavelengths between 200 and 1000 nanometers. The differential reflectograms obtained for various values of d_1, d_2 and $\hat{n}_1$ show a wide variety of curve shapes (see subsections IV-8 through IV-12). Substantial structure is observed in these graphs. As will be shown herein, the structure contains the desired information about thickness and optical properties of the film.

IV-5 Simplification of Equations

Equations (4-12) through (4-15), (4-17), (4-18) and (4-22) lack easy visualization of how the spectrum varies as a function of wavelength or frequency. It is possible however, to alter equation (4-22) into a pure real expression. This is accomplished by assuming that k_1 is small. The derivation listed in Appendix A, subsection A-4, yields the following expression

$$\frac{\Delta R}{\bar{R}} = \frac{2\sin(2\pi n_1(d_1-d_2)/\lambda)\sin(\varphi+2\pi n_1(d_1+d_2)/\lambda)}{g+\cos(2\pi n_1(d_1-d_2)/\lambda)\cos(\varphi+2\pi n_1(d_1+d_2)/\lambda)} \quad (4\text{-}24)$$

where

n_1 = real part of $\hat{n}_1$, the index of medium "1"

λ = the light wavelength

d_1 = the thickness of medium "1" on one sample side (see Figure 4.1)

d_2 = the thickness of medium "1" on the other sample side (see Figure 4.1)

$$\varphi = \tan^{-1}\frac{\text{Imag}(\hat{P}_{01})}{\text{Real}(\hat{P}_{01})} - \tan^{-1}\frac{\text{Imag}(\hat{T}_{01}\hat{P}_{12}\hat{T}_{10})}{\text{Real}(\hat{T}_{01}\hat{P}_{12}\hat{T}_{10})} \quad (4\text{-}25)$$

$$g = (a^2+f^2)/2af = \frac{|\hat{P}_{01}|^2+|\hat{T}_{01}\hat{P}_{12}\hat{T}_{10}|^2}{2|\hat{P}_{01}||\hat{T}_{01}\hat{P}_{12}\hat{T}_{10}|} \quad (4\text{-}26)$$

$$a = |\hat{P}_{01}| \quad (4\text{-}27)$$

$$f = |\hat{T}_{01}\hat{P}_{12}\hat{T}_{10}| \quad (4\text{-}28)$$

IV-6 Conceptualization of the Simplified Equation

Equation (4-24) is seen to be a pure real expression consisting of a ratio of trigonometric functions of two different arguments. The first argument contains the difference in thickness and the second contains the sum of the thicknesses plus an angle Φ. In addition the denominator contains the factor g. It is possible to understand the general behavior of equation (4-24) by analyzing the numerator and denominator and observing their individual effects upon $\Delta R/\bar{R}$.

The denominator of (4-24) consists of the sum of a factor "g" and a product of two cosine terms with different periods. The maximum range of the cosine product is between plus and minus one. If "g" would assume the value one, the denominator could reach zero, causing an infinite value in equation (4-24). Rearranging (4-26) yields

$$g = (a^2 + f^2)/2af = a/2f + f/2a \quad . \qquad (4\text{-}26a)$$

Let

$$f/a = x \quad . \qquad (4\text{-}29)$$

Then

$$g = 1/2x + x/2 \quad . \qquad (4\text{-}30)$$

Inserting g = 1 yields x = 1. The value of g cannot be negative because it is composed of absolute values, (4-26). A plot of (4-30) shows that g is greater than or equal to unity for all allowable values of x (positive numbers), see figure 4.5. For x = 1, it follows that, from (4-29),

$$f/a = 1$$

or

$$f = a \quad . \tag{4-31}$$

This yields from equations (4-27) and (4-28)

$$\left|\hat{P}_{01}\right| = \left|\hat{T}_{01}\hat{P}_{12}\hat{T}_{10}\right| \tag{4-32}$$

When this condition exists and the wavelength is such that the cosine product term equals minus one, $\Delta R/\bar{R}$ goes to infinity. Inspection of the cosine product term shows that it may reach minus one only if $\Phi = 0$ and either $d_1 = 0$ or $d_2 = 0$.

The value of Φ, defined by equation (4-25), will not be zero for the cases under consideration. Therefore the cosine product will not equal minus one. For the product to take on values close to minus one, the periods must be very different such that one cosine term is nearly one (or minus one) while the other periodically goes from one to minus one. This condition occurs when d_1 is small.

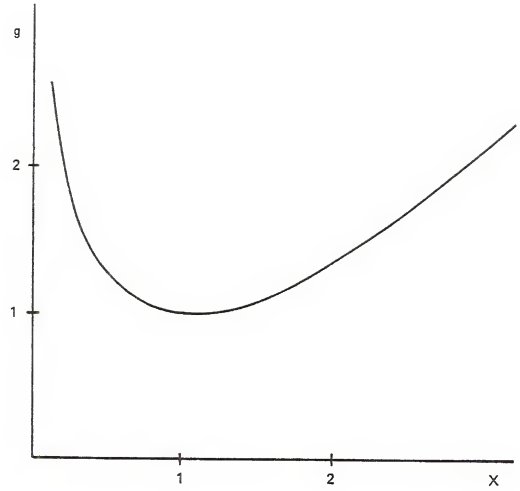

Figure 4.5 Variation of $g = (a^2 + f^2)/2af$ as a function of $x = f/a$.

This causes the following:

$$\cos(2\pi n_1(d_1 - d_2)/\lambda) \text{ is close to } +1 \text{ or } -1 \quad (4\text{-}33)$$

and additionally

$$\cos(\varphi + 2\pi n_1(d_1+d_2)/\lambda) \text{ rapidly varies between } +1 \text{ and } -1 \; . \quad (4\text{-}34)$$

Thus the value of $\Delta R/\bar{R}$ may reach large but not infinite values under the conditions of (4-32) and

$$d_1 \text{ close to } d_2 \quad . \quad (4\text{-}35)$$

The numerator of (4-24) forces the value of $\Delta R/\bar{R}$ to zero whenever either of the two sine terms is equal to zero. This occurs when

$$2\pi n_1(d_1-d_2)/\lambda_{i1} = m_1\pi \quad , \; m_1 = \text{integer} \quad . \quad (4\text{-}36)$$

The numerator is also zero when

$$\varphi + 2\pi n_1(d_1+d_2)/\lambda_{i2} = m_2\pi \quad , \; m_2 = \text{integer}. \quad (4\text{-}37)$$

Solving (4-36) and (4-37) for the wavelengths at which the numerator is zero and hence $\Delta R/\bar{R}$ is zero yields

$$\lambda_{i1} = 2n_1(d_1 - d_2)/m_1 \quad , \quad m_1 = \text{integer} \quad , \qquad (4\text{-}38)$$

$$\lambda_{i2} = 2n_1(d_1 + d_2)/(m_2 - \Phi/\pi) \quad , \quad m_2 = \text{integer}. \qquad (4\text{-}39)$$

Equation (4-24), when programmed, generates data that closely match the results of the original equation, (4-22) as long as the conditions of equation (A-31 of appendix A are maintained. It should be mentioned however that the exact equation (4-22) was used for all calculations and plots. Equation (4-24) is less accurate but it is much easier to conceptualize. Hence (4-24) is used primarily in rationalizing the results and in pointing the way to solutions.

IV-7 Results of the Calculations

Line-shape analysis of the calculated differential reflectograms was employed to gain new insights into experimental differential reflectograms of the tungsten/tungsten-oxygen system. By comparing the experimental and theoretical results it is possible to identify interband as well as interference peaks and to quantify the differential reflectometry analysis. Additionally, a number of further metal/metal-oxygen systems were investigated to demonstrate that the method is generally applicable.

IV-8 Calculated Differential Reflectograms, Thickness Effects

The possible wavelength range of the calculated differential reflectograms is from zero to infinity. The experimental range is, however, only from 200 to 800 nm. Plotting the calculated DR spectra at both a wide range and a range corresponding to the experimental reflectograms gives a more comprehensive insight into the problem at hand.

Figure 4.6 shows calculated differential reflectograms ($\Delta R/\bar{R}$ as a function of λ) for transparent dielectric films on a metal substrate. The thicknesses, d_1 and d_2, of the two transparent adjacent layers are assumed to be different, Figure 4.1. The thickness d_1 varies in the three curves of Figure 4.6, whereas d_2 remains small and constant. The optical constants are noted in the figure caption. The wavelength range was chosen to be from 0 to 5000 nm. The calculations were performed using equations (4-12)through (4-15) and (4-17), (4-18) and (4-22). The computer program is contained in Appendix D.

Inspection of Figure 4.6 reveals that at low photon energies (long wavelengths) the differential reflectivity is relatively constant and structureless. At high photon energies (shorter wavelengths) pronounced maxima and minima develop which have the appearance of interference type oscillations. The first maximum (moving along the horizontal axis toward higher energies) shifts to lower energies with increasing thickness, d, of the dielectric film.

Figure 4.6 Calculated differential reflectograms of a metal oxide on a metal substrate. The sample configuration is shown in Figure 4.1. The value of d_1 increases from curve (a) through (c) and d_2 is 0.1 nm. The values of the optical constants were taken to be, $\hat{n}_0 = 1$, $\hat{n}_1 = 1.6 - i\ 2 \times 10^{-6}$ and $\hat{n}_2 = 3 - i\ 3$.

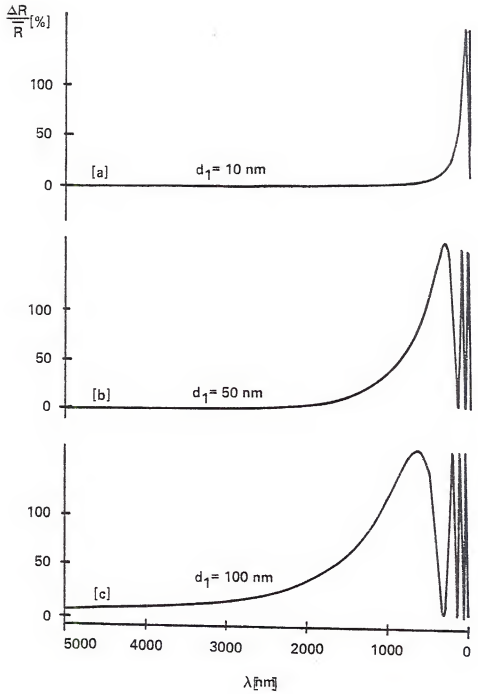
ΔR/R [%]
100
50
0
[a]
d1 = 10 nm
100
50
0
[b]
d1 = 50 nm
100
50
0
[c]
d1 = 100 nm
5000
4000
3000
2000
1000
0
λ [nm]

This can also be seen from equation (4-24) by setting $d_2 = 0$.

$$\frac{\Delta R}{\bar{R}} = \frac{2 \sin(2\pi n_1 d_1/\lambda) \sin(+2\pi n_1 d_1/\lambda)}{g + \cos(2\pi n_1 d_1/\lambda) \cos(+2\pi n_1 d_1/\lambda)} \qquad (4\text{-}40)$$

In Figure 4.7 the same specimen configuration as before was assumed; however, the wavelength range for which the differential reflectograms were calculated was taken to be between 200 and 1000 nanometers, which more closely resembles the range for the experimental reflectograms shown later in this section. Similar structure, as seen in Figure 4.6, can be observed. Again the structure is more pronounced the thicker the dielectric film, d_1, assumed.

Inspection of equation (4-24) reveals that the first peak comes mainly from the term

$$\sin(\varphi + 2\pi n_1(d_1 + d_2)/\lambda) \quad . \qquad (4\text{-}41)$$

This is true because at large wavelengths the cosine terms are nearly unity and the sine terms are nearly zero. As λ becomes smaller, the value of (4-41) grows the fastest. It approaches values significantly greater than zero as:

$$\varphi = 2\pi n_1(d_1 + d_2)/\lambda \quad . \qquad (4\text{-}42)$$

Figure 4.7 Calculated differential reflectograms of a metal oxide on a metal substrate. The sample configuration is shown in Figure 4.1. The value of d_1 increases from curve (a) through (e) and d_2 is 0.1 nm. The values of the optical constants were taken to be $\hat{n}_0 = 1$, $\hat{n}_1 = 1.6 - i\ 2 \times 10^{-6}$ and $\hat{n}_2 = 3 - i\ 3$.

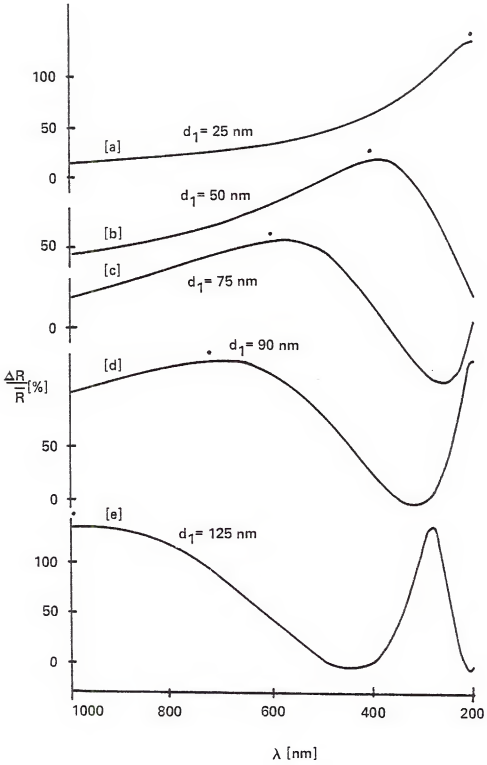
100
50
0
[a]
d_1= 25 nm
d_1= 50 nm
[b]
50
[c]
d_1= 75 nm
0
d_1= 90 nm
[d]
$\frac{\Delta R}{R}$[%]
50
0
[e]
d_1= 125 nm
100
50
0
1000
800
600
400
200
λ [nm]

However it has been observed that the peak position is primarily a function of the greater of the two thicknesses. Considering this fact yields

$$\Phi \cong 2\pi n_1 d_m / \lambda_p \quad .$$

Solving for λ_p yields

$$\lambda_p \cong 2\pi n_1 d_m / \Phi \quad . \tag{4-43}$$

Referring to (4-25) the value of Φ is dependent upon the particular optical constants. A typical value is $2\pi/5$. This yields

$$\lambda_p \cong 5\, n_1\, d_m \quad , \tag{4-44}$$

where

λ_p is the approximate position of the lowest energy (longest wavelength) interference peak, and

d_m is the larger of the two thicknesses, d_1 and d_2.

Equation (4-44) gives a value of λ in the vicinity of the first peak. As n_1 increases and as d_m increases, the position of the first peak moves to lower energies, longer wavelengths. Thus the condition under which

geometric peaks will nor appear in the differential reflectogram is for a low $n_1 \times d_m$ product.

The shortest wavelength in the experimental differential reflectograms is 200 nm. If all interference peaks are required to be at a shorter wavelength than 200 nm then

$$n_1 d_m < 40 \text{ nm} \quad . \tag{4-45}$$

For WO_3, n_1 is 2.45 which yields

$$d_m < 16 \text{ nm} \quad . \tag{4-45a}$$

So as long as the WO_3 film is less than 16 nm thick, no interference peaks will occur in the differential reflectogram. Figure 4.7 shows the expected peak position as calculated by equation (4-44).

IV-9 Effect of n_1 Variation

The calculated differential reflectograms presented in Figure 4.8 assume a sample configuration as shown in Figure 4.1. The value of n_1 varies from curve (a) through (f). Other parameters are indicated in the caption of the figure. It can be seen that the effect of increasing n_1 is similar to that of increasing the thickness, see Figure 4.7. This also can be deduced by inspecting equation (4-24)

Figure 4.8 Calculated differential reflectograms of a metal oxide on a metal substrate. The sample configuration is shown in Figure 4.1. The value of n_1 is varied from curve (a) through (f) as indicated in the figure. The value of the optical constants were taken to be $\hat{n}_0 = 1$, $\hat{n}_2 = 3 - i\,3$ and $k_1 = 2 \times 10^{-6}$. The thicknesses were $d_1 = 20$ nm and $d_2 = 10$ nm.

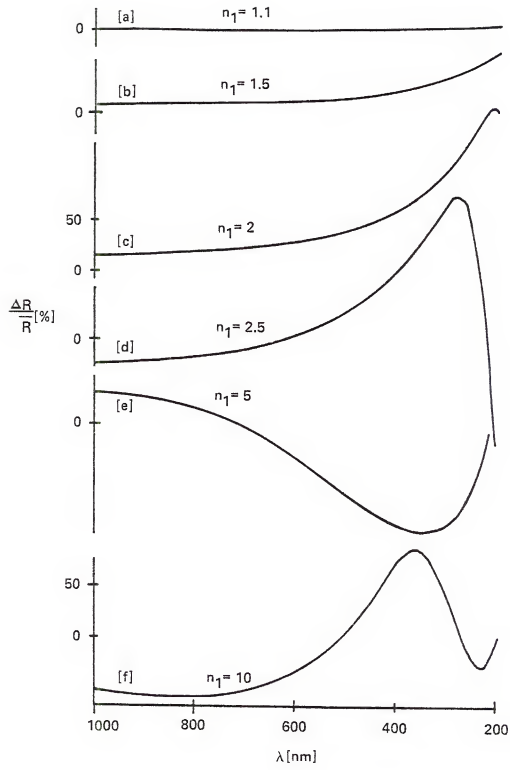
[a]
n_1= 1.1
0
[b]
n_1= 1.5
0
50
[c]
n_1= 2
0
$\frac{\Delta R}{R}$[%]
0
[d]
n_1= 2.5
0
[e]
n_1= 5
50
0
[f]
n_1= 10
1000
800
600
400
200
λ[nm]

in which thickness d and n_1 are products in the arguments of the sine and cosine terms.

Refer also to the results presented in subsection IV-12 in which changes in peak shape can be seen when n_1 is varied and the difference in thickness $(d_1 - d_2)$ is small.

IV-10 Effect of k_1 Variation

The calculated differential reflectograms of Figure 4.9 result from a sample as shown in Figure 4.1. The value of k_1 increases from (a) through (f). Other parameters are indicated in the caption of the figure. The curve is virtually unaffected by increasing k until the value of k_1 has changed five orders of magnitude, curve (d). Inspection of equation (A-25), along with (A-31) of Appendix A, provides an explanation of this effect. As long as the inequality of equation (A-31) is maintained, the value of k_1 can be expected to have a negligible effect on the differential reflectogram. When the inequality is no longer met, equation (A-25) can be seen to approach the following as k_1 increases further:

$$\left| \frac{\hat{E}_{d1}}{\hat{E}_i} \right| = a^2 \quad . \tag{4-46}$$

Similarly

Figure 4.9 Calculated differential reflectograms of a metal oxide on a metal substrate. The sample configuration is shown in Figure 4.1. The optical constants were taken to be $\hat{n}_0 = 1$, $n_1 = 2.5$ and $\hat{n}_2 = 3 - i\,3$. The value of the imaginary part of $\hat{n}_1$ was varied as shown on the figure, k_1. The thicknesses were $d_1 = 20$ nm and $d_2 = 10$ nm.

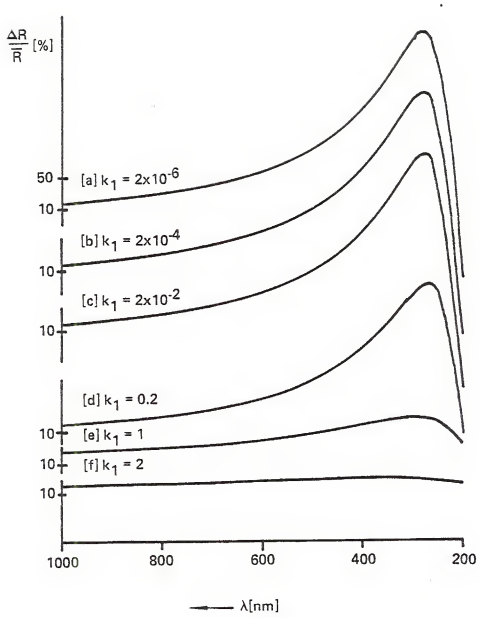
ΔR/R [%]
50
10
[a] k1 = 2x10-6
[b] k1 = 2x10-4
10
[c] k1 = 2x10-2
10
[d] k1 = 0.2
10
[e] k1 = 1
10
[f] k1 = 2
10
1000
800
600
400
200
λ[nm]

$$\left| \frac{\hat{E}_{d2}}{\hat{E}_i} \right| = a^2 \quad . \tag{4-47}$$

Substitution into (4-21) yields

$$\frac{\Delta R}{\bar{R}} = 0 \tag{4-48}$$

Consequently as k_1 increases, initially there is no significant effect upon the differential reflectogram. As k_1 increases, the differential reflectogram amplitudes are reduced toward zero.

IV-11 Spectral Range Without Interference Peaks

It now has been demonstrated that interference-type oscillations observed in the differential reflectograms presented in Figures 4.6 - 4.9 are entirely caused by the geometry of the specimens as shown in Figure 4.1. The observed peaks are neither due to a change in optical properties with wavelength (dispersion) nor interband transitions. Therefore it is important to identify the conditions for which these geometric peaks can be eliminated or at least minimized in the spectral range used for experimental investigations, i. e. between 200 and 800 nm.

There are two possible ways to limit the influence of the interference peaks. One is to prepare specimens

such that the interference peaks all occur at wavelengths below 200 nm. The other is to prepare specimens so that the amplitude of the interference peaks in the spectral range is minimized.

Equation (4-45) contains the conditions under which the interference peaks will all fall to shorter wavelengths than the minimum of the spectral renge, namely 200 nm.

$$n_1 d_m < 40 \text{ nm} \qquad (4\text{-}45)$$

If equation (4-45) cannot be satisfied because both n_1 and d_m are large, then the amplitude of the interference peaks which will occur in the spectral range can be minimized by minimizing the difference in thickness between the two specimen halves. Figure 4.10 shows calculated differential reflectograms for samples represented by Figure 4.1. The value of d_1 is constant at 500 nm while d_2 increases steadily in curves (a) through (d). It can be seen that the peak heights are reduced as the difference in thickness ($d_1 - d_2$) becomes smaller.

It can be shown that the greatest peak amplitude may be restricted to a maximum value, D, under the following conditions; see Appendix C,

$$n_1(d_1 - d_2)/\lambda < F \qquad (4\text{-}49)$$

Figure 4.10 Calculated differential reflectograms of a metal oxide on a metal substrate. The sample configuration is shown in Figure 4.1. The thickness of the two sample sides is indicated on the curves. The values of the optical constants were taken to be $\hat{n}_0 = 1$, $\hat{n}_1 = 1.6 - i\ 2 \times 10^{-6}$ and $\hat{n}_2 = 3 - i\ 3$.

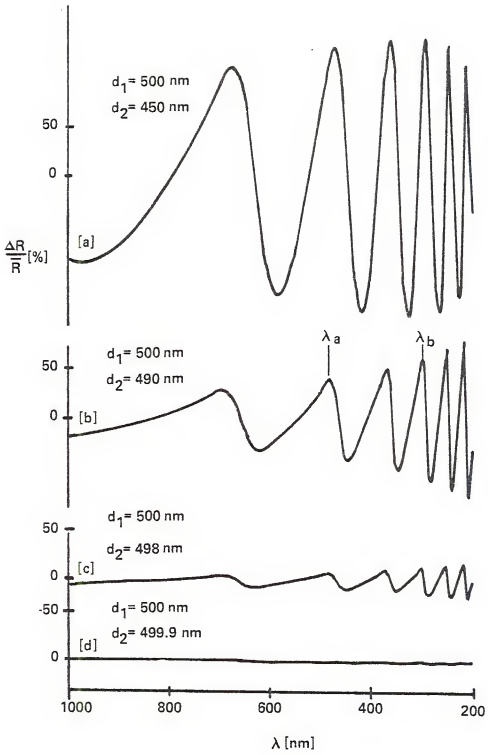
d1= 500 nm
d2= 450 nm
50
0
[a]
ΔR/R [%]
λa
λb
d1= 500 nm
d2= 490 nm
50
0
[b]
d1= 500 nm
d2= 498 nm
50
0
[c]
-50
d1= 500 nm
d2= 499.9 nm
[d]
0
1000
800
600
400
200
λ [nm]

where

$$F = (1/2\pi) \sin^{-1} (2D) \qquad (4\text{-}50)$$

and

$$g \rangle 1.2 \quad . \qquad (4\text{-}51)$$

IV-12 Interference Peak Shapes

Figure 4.11 shows calculated differential reflectograms assuming the difference in thickness between two transparent films to be one nanometer (d_1 = 50 nm and d_2 = 49 nm). The The value of n_1 increases from curve (a) through (d). The other optical parameters are listed in the figure caption. The value of "g" was calculated from equation (4-26) and is listed on the figure. Recall that "g" is a strict function of $\hat{n}_0$, $\hat{n}_1$ and $\hat{n}_2$. Thus the variation in "g" results from the variation in n_1. Figure 4.11 reveals that the interference peaks become more pronounced when "g" approaches unity. This confirms the result already discussed in subsection IV-6 stating that the peak shape and size may change when "g" is close to unity and the difference in thickness between the two oxide layers is small. The result of subsection IV-9 which shows that the peak position is dependent upon n_1 is also confirmed.

The significance of this result is that it may permit an estimate of n_1 from experimental differential reflectograms if both $\hat{n}_0$ and $\hat{n}_2$ are known and the peaks are

Figure 4.11 Calculated differential reflectograms of a metal oxide on a metal substrate. The sample configuration is shown in Figure 4.1. The value of the real part of $\hat{n}_1$ (n_1) is varied as shown from curve (a) through (d). The optical constants were taken to be $\hat{n}_0 = 1$, $k_1 = 2 \times 10^{-6}$ and $\hat{n}_2 = 3 - i\,3$. The thicknesses were $d_1 = 50$ nm and $d_2 = 49$ nm.

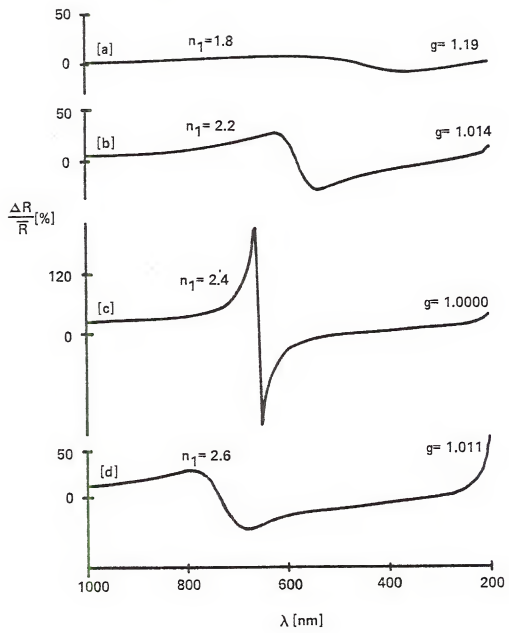
50
0
[a]
n_1=1.8
g= 1.19
50
0
[b]
n_1= 2.2
g= 1.014
$\frac{\Delta R}{R}$[%]
120
0
[c]
n_1= 2.4
g= 1.0000
50
0
[d]
n_1= 2.6
g= 1.011
1000
800
600
400
200
λ [nm]

pronounced as shown in Figure 4.11, curve (c). The estimate is made by comparing calculated differential reflectograms for various values of n_1 with the experimental differential reflectograms. The value of n_1 which yields a close match is taken to be an estimate of n_1 in the experimental case. An example of this is presented in subsection IV-14.

IV-13 Theoretical Reflectogram Summary

Table 4.1 summarizes the effects of the basic parameters upon calculated differential reflectograms. Equations are shown in the table.

IV-14 Tungsten Oxide

Figure 4.12 shows experimental differential reflectograms of tungsten oxide films on a tungsten substrate. The specimens were produced by the method described in Section III and have the configuration of Figure 4.1, i. e. the thickness of the oxide on the two sample halves is different. It was observed that both sample halves of each sample show visible coloration resulting from interference effects. This verifies that some oxide is present on each half after polishing. The sample was polished to bare metal after each corrosion treatment.

TABLE 4.1

Summary of results obtained for calculated differential reflectograms of thin film corrosion products on a metal substrate as vital parameters of the film are varied.

variation of parameter	results of $d_2 \to 0$ & $0 < d_2 < d_1$	results if $(d_1 - d_2)$ is small
if d_1 increases	peaks move to longer λ (lower energies) $\lambda_p = 5 n_1 d_m$	same
if n_1 increases	peaks move to longer λ (lower energies) $\lambda_p = 5 n_1 d_m$	same and peak shapes may change
if k_1 increases	peak positions virtually unaffected as long as $k_1 d_m/\lambda < (-\ln(1-E))/4$, otherwise amplitude is reduced	same
if $(d_1 - d_2)$ decreases	the maximum amplitude is reduced $n_1(d_1-d_2)/\lambda < (1/2\pi)\sin^{-1} 2D$	same if $g > 1.2$ otherwise the maximum amplitude is arbitrarily reduced

Figure 4.12 Experimental differential reflectograms of tungsten oxides on tungsten substrates. each curve has been obtained by heating a tungsten sample in dry oxygen for 20 minutes to the final temperature indicated on the curve. Part of the oxide is removed from half of the specimen as described in Section III to produce a sample configuration shown in Figure 4.1

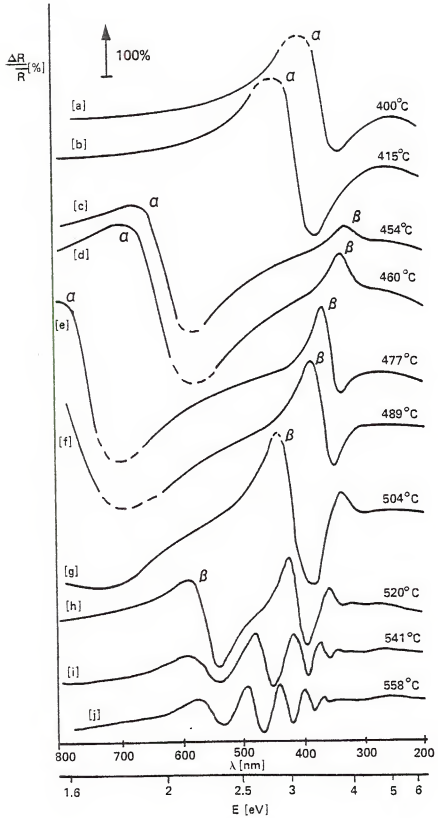
ΔR/R [%]
100%
[a]
[b]
[c]
[d]
[e]
[f]
[g]
[h]
[i]
[j]
α
β
400°C
415°C
454°C
460°C
477°C
489°C
504°C
520°C
541°C
558°C
800
700
600
500
400
300
200
λ [nm]
1.6
2
2.5
3
4
5
6
E [eV]

Curve (a) of Figure 4.12 was obtained by annealing tungsten metal for twenty minutes at 400 °C in a pure, dry oxygen atmosphere. Starting from low photon energies curve (a) shows a gradual rise in $\Delta R/\bar{R}$ with a maximum, termed peak α, around 400 nm. A minimum exists at 385 nm and a broad flat maximum around 242 nm. The differential reflectogram represented in (b) of Figure 4.12 was obtained by annealing tungsten at 415 °C similarly as above. A shift of the position of peak α to smaller photon energies is evident. With increasing annealing time the peaks are shifted further toward lower photon energies and new peaks emerge. For example, in Figure 4.12 curve (c), a peak appears at 325 nm and is termed peak β. The peak structure observed in Figure 4.12 is interpreted to be caused by interference effects resulting from the slightly absorbing film on the absorbing substrate as discussed in subsection IV-3. See Figure 4.2.

The curves obtained by annealing below 520 °C, (a) through (g), exhibit a sharpened peak shape as discussed in subsection IV-6. This peak shape indicates a value of n_1 in the vicinity of 2.5, see Figure 4.11. This is in agreement with the value of Sawada and Danielson[56] who found $n_1 = 2.45$ for tungsten trioxide, see subsection II-8. Starting with the curve obtained by annealing tungsten at 520 °C, Figure 4.12 (h), the interference pattern changes in sequence and shape. More peaks

emerge which appear more sinusoidal and have a reduced amplitude. This coincides with the formation of new oxides above 484 °C. See the tungsten-oxygen phase diagram presented in Figure 2.13.

IV-15 Interband Transition Peaks

One of the goals of this study is to establish characteristic differential reflectograms for thin film corrosion products. As shown elsewhere,[21] differential reflectograms of corrosion products on metal substrates are distinguished by certain maxima and minima which are caused by electron transitions between filled lower and unfilled upper energy states.

Calculated electron band structures, if available, allow positive identification of the peaks in the differential reflectograms. The previous sections demonstrate that in addition to peaks caused by interband transitions, interference peaks may be observed in the reflectograms if the oxide thickness is within a certain range. It has been shown in subsection IV-8 that differential reflectograms will not contain interference peaks if the n x d product is less than 40 nm, equation (4-45). They will, however, contain the gentle rise in $\Delta R/\bar{R}$ towards higher photon energies that is the shoulder of an interference peak occuring off scale to higher energies, Figure 4.13.

Figure 4.13 depicts an experimental differential reflectogram for tungsten trioxide on a tungsten substrate which was obtained by annealing tungsten for twenty minutes at 251 °C and removing a thin layer of oxide from half of the sample as described in Section III. An upward trend in $\Delta R/\bar{R}$ toward higher photon energies is observed as discussed above.

Superimposed on this curve is an ε_1 type peak structure[70] which is interpreted to be caused by interband transitions. For an ε_1 type structure the characteristic energy, E_t, for an electron interband transition is in the center between the maximum and minimum. From Figure 4.13, E_t can be found to be 4.54 eV (273 nm). This value corresponds to one of the transitions as seen in Figure 2.14 at the M symmetry point.

Figure 4.14 shows a differential reflectogram taken on molybdenum oxide grown on a molybdenum substrate following the experimental procedure previously described. The curve shows the familiar upward trend toward higher photon energies. Superimposed on this curve are two very weak ε_2 type peaks which are observable by extending the base line below the curve. These peaks are at approximately 3.74 eV (330 nm) and 4.95 eV (250 nm). Band diagrams for molybdenum oxides have not yet been published.

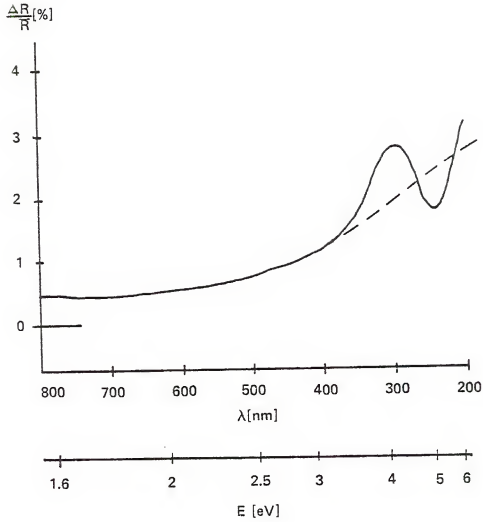

Figure 4.13 Experimental (——) and calculated (---) differential reflectograms of tungsten trioxide on a tungsten substrate. The specimen has been annealed to 251 °C in dry oxygen for twenty minutes. Part of the corrosion product was removed from half of the specimen by the technique described in Section III. The calculated curve assumes multiple internal reflections.

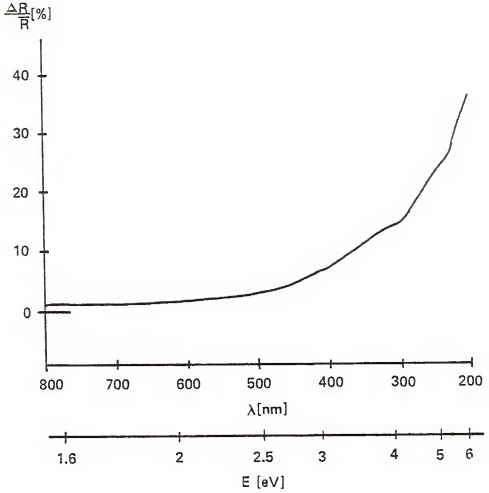

Figure 4.14 Experimental differential reflectogram of molybdenum oxide on a molybdenum substrate. The specimen is produced by heating molybdenum to 348 °C in dry oxygen for twenty minutes. Part of the oxide is removed from half of the specimen by the technique of Section III to obtain a sample configuration of Figure 4.1.

Figure 4.15 presents a differential reflectogram of chromium oxide on a chromium substrate as described before. Four peaks are visible at 6.0 eV (206 nm), 5.31 eV (233 nm), 4.0 eV (310 nm) and 3.3 eV (375 nm). Annealing the specimen at various temperatures up to 648 °C yields the same four peak positions and the emergence of an underlying, broad interference maximum which moves toward longer wavelengths with increasing temperature. Thus the four peaks just listed are identified as being due to interband transitions and the broad maximum (not seen in Figure 4.15) as due to interference effects.

Figure 4.16 presents differential reflectograms of copper oxides on copper substrates prepared the same way as before. Five peaks are evident in the lower curve of Figure 4.16 at 2.21 eV (560 nm), 2.75 eV (450 nm), 3.21 eV (385 nm), 3.85 eV (321 nm) and 5.11 eV (242 nm). These peaks agree quite well with those previously reported by Shanley et al. who reported peaks at 560 nm, 455 nm, 380 nm, 314 nm and 237 nm for copper which had been oxidized by electrochemical means.[21] The upper reflectogram (CuO) shows structure around 2.2 eV (550 nm) and 3.9 eV (320 nm) also in agreement with the data of Shanley.[8] This comparison demonstrates that electrochemical oxidation and high temperature oxidation in dry oxygen yield the same differential reflectograms for copper.

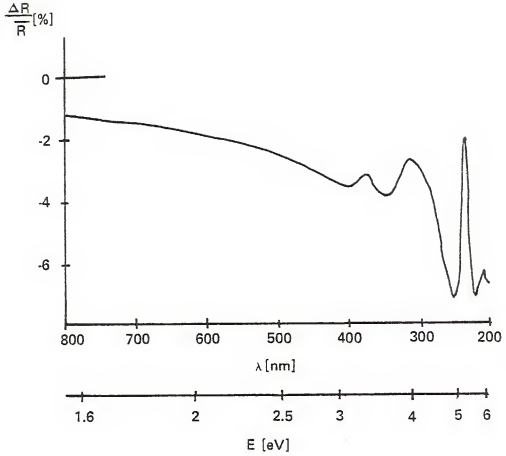

Figure 4.15 Experimental differential reflectogram of chromium oxide on a chromium substrate. The specimen was heated to 470 °C in dry oxygen for twenty minutes. Part of the corrosion product was removed from half of the specimen by the method of Section III to produce a sample configuration of Figure 4.1.

Figure 4.16 Experimental differential reflectograms of copper oxides on copper substrates. The top curve is representative of CuO and was produced from a specimen of copper, heated to 106 °C for 8 minutes in oxygen. Part of the oxide is removed from half of the specimen as described in Section III to produce a sample configuration shown in Figure 4.1. The lower curve is representative of Cu_2O and was produced by heating copper to 144 °C for 18 minutes in dry oxygen. The oxide was partly removed as above.

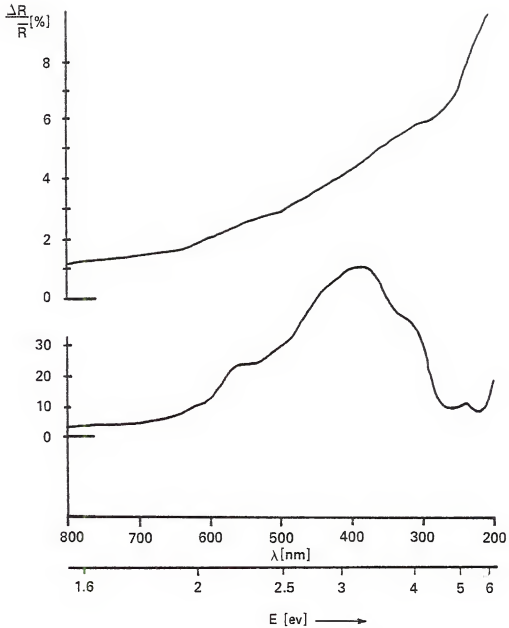
ΔR/R [%]
8
6
4
2
0
30
20
10
0
800
700
600
500
400
300
200
λ [nm]
1.6
2
2.5
3
4
5
6
E [ev]

Figures 4.17 and 4.18 present differential reflectograms of the magnesium-oxygen and zinc-oxygen systems. Both were prepared as described as above. Neither shows discernible interband transition peaks. The curve shape which is evident in both cases is due to interference. It is possible that these films are amorphous and hence do not exhibit transitions caused by band structure.

IV-16 Obtaining k and d

In order to obtain k and d values from the experimental results, a match of the experimental curves with the calculated curves is necessary. This is accomplished by obtaining a differential reflectogram from a metal-oxide system in which the values of the optical constants of the metal substrate and the surrounding medium (e. g. air) already are known. To simplify the process the specimen is prepared with a thin film of oxide covering metal on one sample half and bare metal on the other half, see Figure 1.1. This effectively eliminates the second thickness value from consideration.

Figure 4.13 presented in subsection IV-15 has been obtained on the tungsten-oxygen system as previously described. The sample was prepared so that one side was bare metal and the other was covered with a film which is sufficiently thin so that both interband and interference information is present. Good correspondence

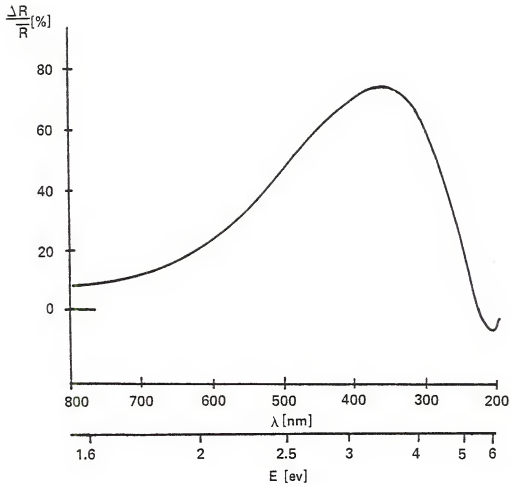

Figure 4.17 Experimental differential reflectogram of magnesium oxide on a magnesium substrate. The specimen was prepared by annealing magnesium to 54 °C for five minutes in dry oxygen. Part of the oxide was removed by the techniques of Section III to obtain the configuration of Figure 4.1.

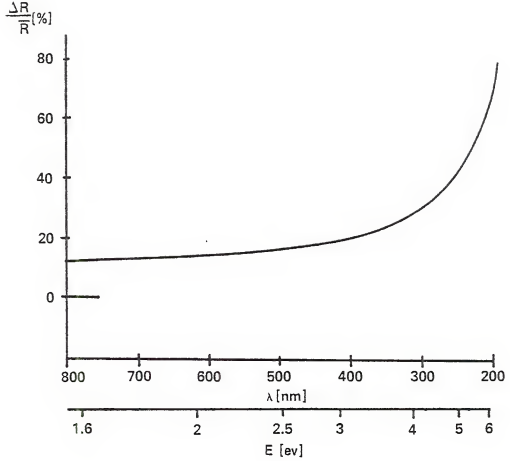

Figure 4.18 Experimental differential reflectogram of zinc oxide on a zinc substrate. The specimen was prepared by annealing zinc to approximately 340 °C for 35 minutes in dry oxygen. Part of the oxide was removed from half of the specimen by the methods of Section III to obtain the sample configuration of Figure 4.1.

with theory was obtained when the value of n_1 of Sawada and Danielson[56] of 2.45 was selected. The values of the film thickness, d, and absorption coefficient, k, were adjusted to obtain a calculated reflectogram as represented by the dashed line on Figure 4.13 using the multiple internal reflections equations of Appendix B. The values of k and d which produced the match were k = 2.2 and d = 2.8 nm. The difference between the experimental and calculated differential reflectograms of Figure 4.13 are considered to be due to the contribution of interband transitions in the oxide layer.

IV-17 Effect of Film Thickness on Signal Strength, $\Delta R/\bar{R}$

In Figures 4.19 through 4.28 curves of $\Delta R/\bar{R}$ versus oxide film thickness are shown assuming the sample configuration of Figure 1.1. The wavelength is 650 nanometers. Optical parameters are indicated on the figures and in the captions. If the optical constants of a sample are known it is possible to estimate the film thickness from the appropriate figure.

Observe that two figures are presented for each combination of optical parameters. These are each calculated according to both the single internal reflection equation and the multiple internal reflection equation. Appendix B discusses the differences between the two equations.

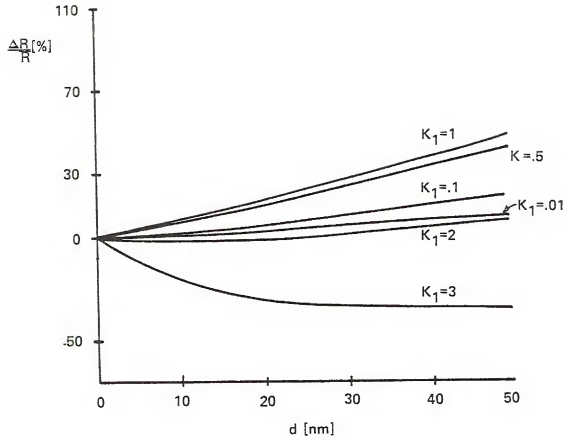

Figure 4.19 Calculated value of $\Delta R/\bar{R}$ versus the thickness of an oxide film on a metal substrate assuming the sample configuration of Figure 1.1. A single internal reflection was assumed. The values of the optical constants were taken to be $\hat{n}_0 = 1$, $n_1 = 1.1$ and $\hat{n}_2 = 3 - i\,3$. The values of k_1 are indicated on the figure. The wavelength is 650 nanometers.

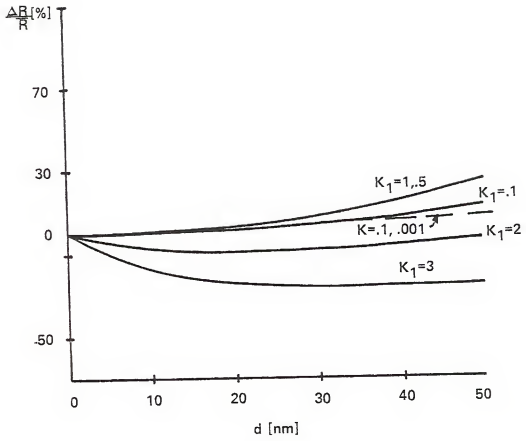

Figure 4.20 Calculated value of $\Delta R/\bar{R}$ versus the thickness of an oxide film on a metal substrate assuming the sample configuration of Figure 1.1. Multiple internal reflections were assumed. The values of the optical constants were taken to be $\hat{n}_0 = 1$, $n_1 = 1.1$ and $\hat{n}_2 = 3 - i\,3$. The values of k_1 are indicated on the figure. The wavelength is 650 nanometers.

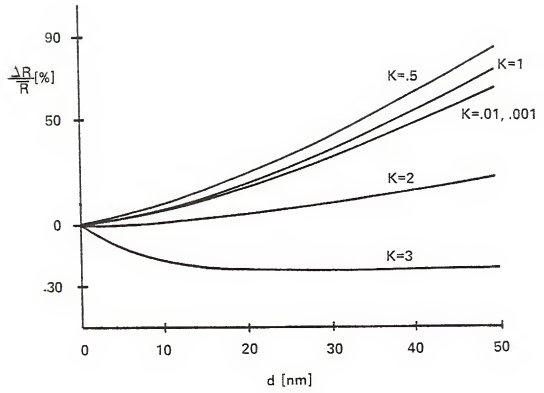

Figure 4.21 Calculated value of $\Delta R/\bar{R}$ versus the thickness of an oxide film on a metal substrate assuming the sample configuration of Figure 1.1. A single internal reflection was assumed. The values of the optical constants were taken to be $\hat{n}_0 = 1$, $n_1 = 1.5$ and $\hat{n}_2 = 3 - i\,3$. The values if k_1 are indicated on the figure. The wavelength is 650 nanometers.

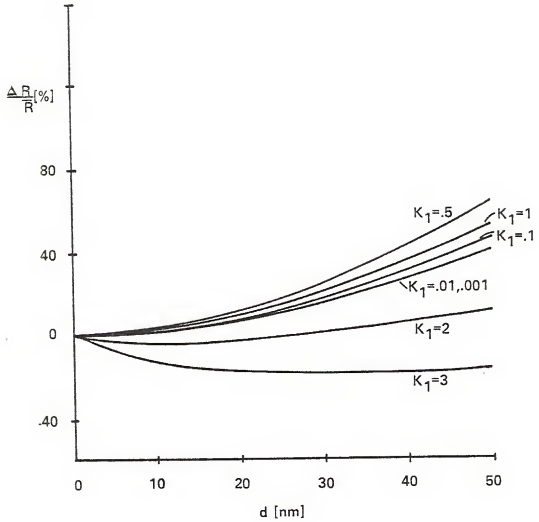

Figure 4.22 Calculated value of $\Delta R/\bar{R}$ versus the thickness of an oxide film on a metal substrate assuming the sample configuration of Figure 1.1. Multiple internal reflections were assumed. The values of the optical constants were taken to be $\hat{n}_0 = 1$, $n_1 = 1.5$ and $\hat{n}_2 = 3 - i\,3$. The values of k_1 are indicated on the figure. The wavelength is 650 nanometers.

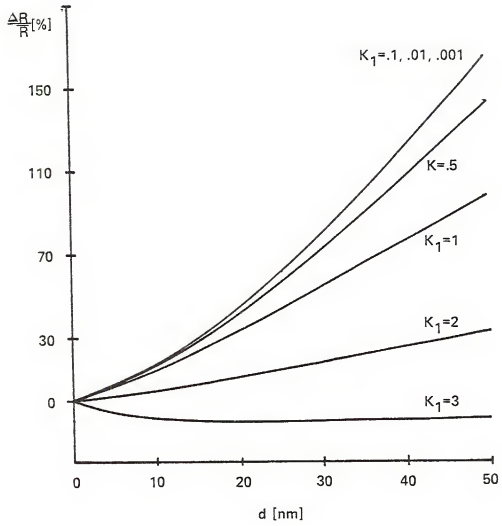

Figure 4.23 Calculated value of $\Delta R/\bar{R}$ versus the thickness of an oxide film on a metal substrate assuming the sample configuration of Figure 1.1. A single internal reflection was assumed. The values of the optical constants were taken to be $\hat{n}_0 = 1$, $n_1 = 2$ and $\hat{n}_2 = 3 - i\,3$. The values of k_1 are indicated on the figure. The wavelength is 650 nanometers.

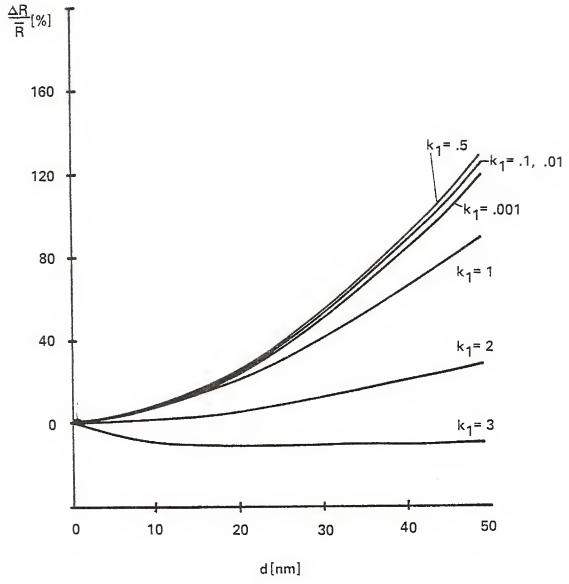

Figure 4.24 Calculated value of $\Delta R/\bar{R}$ versus thickness of an oxide film on a metal substrate assuming the sample configuration of Figure 1.1. Multiple internal reflections were assumed. The values of the optical constants were taken to be $\hat{n}_0 = 1$, $n_1 = 2$ and $\hat{n}_2 = 3 - i\,3$. The values of k_1 are indicated on the figure. The wavelength is 650 nanometers.

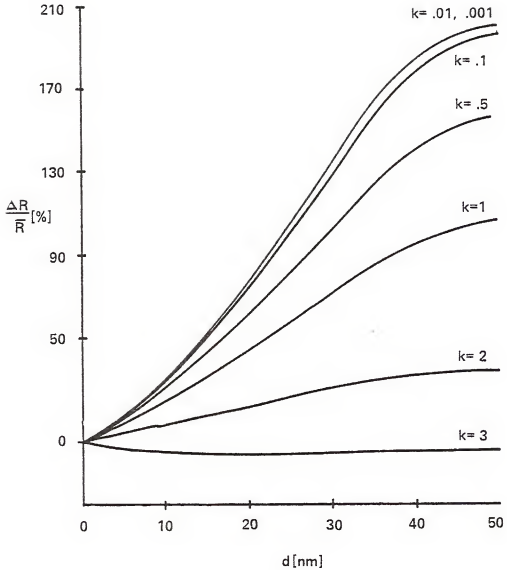

Figure 4.25 Calculated value of $\Delta R/\bar{R}$ versus the thickness of an oxide film on a metal substrate assuming the sample configuration of Figure 1.1. A single internal reflection is assumed. The values of the optical constants were taken to be $\hat{n}_0 = 1$, $n_1 = 2.45$ and $\hat{n}_2 = 3 - i\,3$. The values of k_1 are indicated on the figure. The wavelength is 650 nanometers.

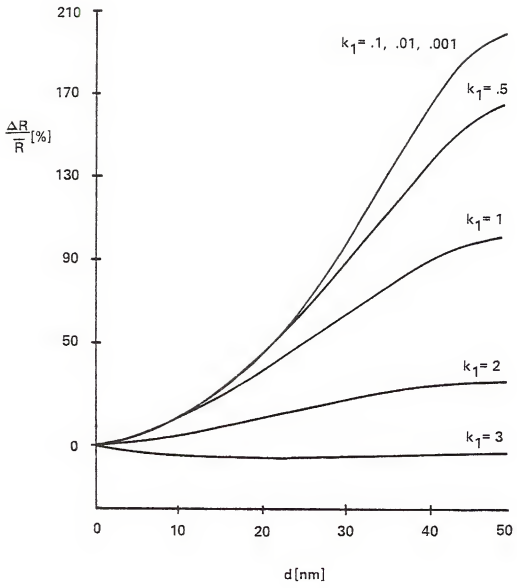

Figure 4.26 Calculated value of $\Delta R/\bar{R}$ versus the thickness of an oxide film on a metal substrate assuming the sample configuration of Figure 1.1. The values of the optical constants were taken to be $\hat{n}_0 = 1$, $n_1 = 2.45$ and $\hat{n}_2 = 3 - i3$. The values of k_1 are indicated on the figure. The wavelength is 650 nanometers.

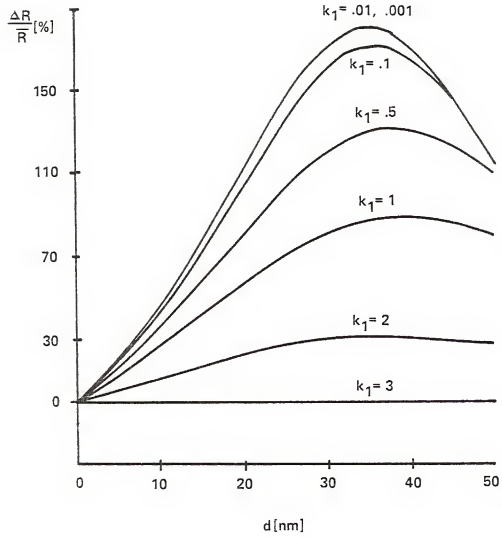

Figure 4.27 Calculated value of $\Delta R/\bar{R}$ versus the thickness of an oxide film on a metal substrate assuming the sample configuration of Figure 1.1. A single internal reflection was assumed. The values of the optical constants were taken to be $\hat{n}_0 = 1$, $n_1 = 3$ and $\hat{n}_2 = 3 - i\,3$. The values of k_1 are indicated on the figure. The wavelength is 650 nanometers.

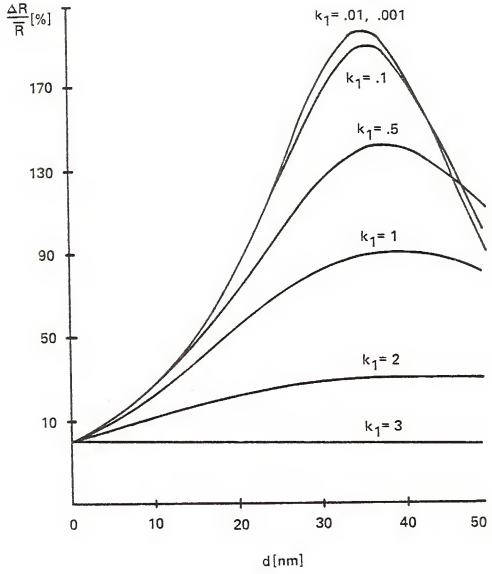

Figure 4.28 Calculated value of $\Delta R/\overline{R}$ versus the thickness of an oxide film on a metal substrate assuming the sample configuration of Figure 1.1. Multiple internal reflections aere assumed. The values of the optical constants were taken to be $\hat{n}_0 = 1$, $n_1 = 3$ and $\hat{n}_2 = 3 - i\,3$. The values of k_1 are indicated on the figure. The wavelength is 650 nanometers.

IV-18 Effect of External Medium Variation

The question naturally arises whether immersing the specimen in a medium other than air may alter the differential reflectogram in a way which aids interpretation. Increasing the index of refraction of the external medium, say by immersing the specimen in oil, will shift the interference peaks to higher energies, possibly moving them off scale to the right. This would simplify identification of interband peaks.

The calculated differential reflectograms presented in Figure 4.29 assume a sample configuration as shown in Figure 4.1. The value of $\hat{n}_0$ is shown on the figure. Other parameters are indicated in the figure caption. It can be seen that increasing the value of $\hat{n}_0$ from 1 + i 0 to 2 + i 0 has the effect of slightly shifting the interference peak to higher energies. The magnitude of the effect, however , is too small to be of value in separating the interband and interference peaks. The value of $\hat{n}_0$ of 2 + i 0 is representative of the higher values obtainable with available oils and hence it may be concluded that further increases in $\hat{n}_0$ would be impractical. Thus while the anticipated effect occurs, it is not of sufficient magnitude to be of practical value in assisting in the interpretation of differential reflectograms.

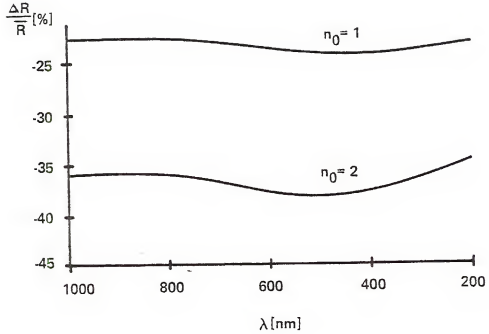

Figure 4.29 Calculated differential reflectograms of a metal oxide on a metal substrate. The sample configuration is shown in Figure 4.1. The value of n_0 is varied as shown on the curves. The value of d_1 = 75 nm and d_2 = 0.01 nm. The values of the other optical constants were taken to be $\hat{n}_1$ = 2.45 - i 2.2 and $\hat{n}_2$ = 3 - i 3.

IV-19 Practical Aspects

It is possible to make a number of general observations from experimental differential reflectograms of metal oxides on metal substrates without performing curve matching.

1. For the case in which n_1 is known, one oxide thickness is essentially zero and the reflectogram exhibits three or more interference peaks, the thickness, d_1, may be found from the reflectogram, (see Appendix F):

$$d_1 = (1/2n_1)(\lambda_a \lambda_b)/(\lambda_a - \lambda_b) \qquad (4\text{-}52)$$

where λ_a and λ_b are defined in Figure 4.10. If n_1 is only known to be within a certain range, an estimate of the thickness may be obtained in the same fashion.

2. If only one interference peak exists in the differential reflectogram, it is possible to estimate the greater film thickness by the following equation derived in subsection IV-8.

$$d_m = \lambda_p / 5\, n_1 \qquad (4\text{-}53)$$

where

λ_p = the peak position and

d_m = the greater of the two oxide thicknesses.

3. The amplitude of the peaks in an experimental reflectogram may be related to the difference in thickness as shown in Appendix C.

$$d_1 - d_2 < (\lambda/2\pi n_1) \sin^{-1} 2D \qquad (4\text{-}54)$$

where

λ = the wavelength at the maximum amplitude and

D = the absolute value of $\Delta R/\bar{R}$ at λ .

Thus if d_2 is effectively zero,

$$d_1 < (\lambda/2\pi n_1) \sin^{-1} 2D \qquad (4\text{-}55)$$

allows an estimate of the largest value possible for d_1.

4. It has been found in the case of thicker oxides, that multiple peaks may occur in only a part of the experimental reflectogram, see Figure 4.12. Preliminary considerations seem to indicate that this may be due to a wavelength dependence of n_1 which allows peaks in the portion of the wavelength range in which n_1 exceeds a critical value and suppresses the peaks elsewhere.

5. A match of the interference features of experimentally obtained reflectograms with a calculated reflectogram is possible under certain conditions.

Firstly the values of the optical constants of the substrate and surrounding medium must be known from 200 to 800 nanometers. Additionally the optical constants of the oxide must be uniform over the 200 to 800 nm range with the exception of narrow band changes attributible to electron interband transitions. And lastly it is helpful though not an absolute necessity if one oxide thickness, d_2, is made experimentally to be near zero to effectively eliminate it as an unknown.

Suspected values of n_1, k_1 and d_1 of the oxide film are entered into the computer program data file and a calculated reflectogram is generated. See Appendix E. By repeated comparison of the experimental and calculated curves it is possible to match them by adjustments in n_1, k_1 and d_1. When a match is obtained, the corresponding parameters are taken to be the constants of the film.

Since the relationship of n_1, k_1 and d_1 with the calculated reflectogram is complicated, see Appendix B, correct adjustments of the parameters may require many attempts. At present no general algorithm exists for performing this in all cases. Each must be considered independently.

6. As a rule, increasing the value of d_1 and/or n_1 moves interference structure to longer wavelengths and reduces the wavelength distance between adjacent peaks. For the case in which no interference peaks appear in the

reflectogram, the result of increases in d_1 and/or n_1 is an upward shift of the curve. If an interference peak exists in the reflectogram, increasing d_1 and/or n_1 moves the peak to longer wavelengths. In this way a discrimination between interference and interband peaks can be achieved. If a number of peaks are evident, increasing d_1 and/or n_1 moves them to smaller photon energies and reduces the spacing between the peaks.

7. Increasing k_1 affects the reflectogram by reducing the amplitude, $\Delta R/\bar{R}$, over the entire wavelength range. The effect is more pronounced at shorter wavelengths. As a consequence, for the case in which no interference peaks are evident, increases in k_1 have the dual effect of reducing the curve amplitude and of tilting the curve downward at the short wavelength end. In the case of several interference peaks, the peak amplitude will be reduced.

SECTION V
CONCLUSIONS AND SUGGESTIONS FOR FUTURE WORK

V-1 Conclusions

1. Experimental differential reflectograms of a metal oxide film of intermediate thickness (more than about 30 nm) contains two types of peaks. One type is caused by interference and the other by electron interband transitions. The separation of interference and interband peaks is possible for these films.

2. For oxide film thicknesses below a critical value (characteristically 30 nanometers), no interference peaks are superimposed on the interband peaks. The interband peaks may be used to identify specific metal oxides on metal substrates since the energies of these characteristic peaks are in reasonable agreement with calculated band diagrams.

3. Differential reflectograms of metal oxide films on metal substrates calculated using the equations of classical electrodynamics are in good agreement with the interference structure found in experimental differential reflectograms.

4. Both calculated and experimental differential reflectograms contain a sequence of interference peaks in addition to interband peaks if the film thickness

multiplied by the film index of refraction is greater than 40 nanometers.

5. The index of refraction, the index of absorption and thickness of the oxide film may be determined from experimental differential reflectograms through the use of line shape analysis.

V-2 Suggestions for Future Work

1. It would be desirable to incorporate a dedicated micro-computer into the differential reflectometer via analog to digital convertors. Experimental differential reflectograms then could be matched quickly with the theoretical model in order to obtain the thickness and optical constants of the film under investigation with a minimum of delay.

2. The computer program should be modified to introduce possible variations of n and k of the metal and metal oxide with light wavelength. By matching the experimental and theoretical differential reflectograms, it may be possible to identify previously unknown variations of optical constants with light wavelength.

3. Detailed investigations of a broader range of metal-oxide systems would lead to a compilation of the characteristic differential reflectograms of thin oxide films. These would facilitate the identification of unknown metal oxide films, for example those forming on alloys or on inter-metallic compounds.

4. For *in situ* corrosion work using the differential reflectometer, one half of the specimen is covered with a transparent, corrosion protective coating. Using the equations derived in this work one could calculate the optical properties of this coating. With this information the choice of the most suitable coating material and thickness should be simplified.

5. The differential reflectometer could be improved by employing a "box-car" integrator or by digital computation of $\Delta R/\bar{R}$. This change would eliminate problems introduced when the waveform produced by the scanning light beam is not perfectly symmetrical.

APPENDIX A
COMPUTER MODEL DERIVATIONS

A-1 Transmission and Reflection Coefficients

As shown by Kraus[71] there exists a relationship between the incident, transmitted and reflected electromagnetic field components tangential to an interface and the properties of the two media composing the interface. From the continuity of the tangential field components at a boundary the following equations can be written, See Figure 4.3,

$$\hat{E}_i + \hat{E}_r = \hat{E}_t \qquad \text{(A-1)}$$

and

$$\hat{H}_i + \hat{H}_r = \hat{H}_t \ . \qquad \text{(A-2)}$$

By definition the electric and magnetic field components of an electromagnetic wave are related by the impedance of the medium in which it propogates.

$$\hat{E}_i \ / \ \hat{H}_i = \hat{Z}_a \qquad \text{(A-3)}$$

and

$$\hat{E}_t \ / \ \hat{H}_t = \hat{Z}_b \qquad \text{(A-4)}$$

Because the reflected wave travels in the negative z direction,

$$\hat{E}_r / \hat{H}_r = -\hat{Z}_a \quad . \tag{A-5}$$

Rearranging (A-3), (A-4) and (A-5) and substituting into (A-2),

$$\hat{H}_t = \hat{E}_t/\hat{Z}_b = \hat{E}_i/\hat{Z}_a - \hat{E}_r/\hat{Z}_a \quad . \tag{A-6}$$

Multiplying by $\hat{Z}_b$,

$$\hat{E}_t = (\hat{Z}_b/\hat{Z}_a)\,\hat{E}_i - (\hat{Z}_b/\hat{Z}_a)\,\hat{E}_r \quad . \tag{A-7}$$

Multiplying (A-1) by $\hat{Z}_b/\hat{Z}_a$,

$$(\hat{Z}_b/\hat{Z}_a)\,\hat{E}_t = (\hat{Z}_b/\hat{Z}_a)\,\hat{E}_i + (\hat{Z}_b/\hat{Z}_a)\,\hat{E}_r \quad . \tag{A-8}$$

Adding (A-7) and (A-8),

$$\hat{E}_t\,(1 + \hat{Z}_b/\hat{Z}_a) = \hat{E}_i\; 2(\hat{Z}_b/\hat{Z}_a) \quad . \tag{A-9}$$

Rearranging gives

$$\hat{E}_t = \hat{E}_i \;\; 2\,\hat{Z}_b/(\hat{Z}_a + \hat{Z}_b) = \hat{E}_i\,\hat{T}_{ab} \quad . \tag{A-10}$$

Where $\hat{T}_{ab}$ is the transmission coefficient,

$$\hat{T}_{ab} = \hat{E}_t/\hat{E}_i = 2\,\hat{Z}_b/(\hat{Z}_b + \hat{Z}_a) \quad . \tag{A-11}$$

Subtracting (A-7) from (A-8) gives

$$\hat{E}_t\,(-1 + \hat{Z}_b/\hat{Z}_a) = \hat{E}_r\,(2\,\hat{Z}_b/\hat{Z}_a) \quad . \tag{A-12}$$

Substituting $\hat{E}_t$ from (A-10) and solving for $\hat{E}_r$ yields

$$\hat{E}_r = \hat{E}_i\,(\hat{Z}_b - \hat{Z}_a)/(\hat{Z}_b + \hat{Z}_a) = \hat{E}_i\,\hat{P}_{ab} \quad . \tag{A-13}$$

Where $\hat{P}_{ab}$ is the transmission coefficient

$$\hat{P}_{ab} = \hat{E}_r/\hat{E}_i = (\hat{Z}_b - \hat{Z}_a)/(\hat{Z}_b + \hat{Z}_a) \quad . \tag{A-14}$$

The subscripts of $\hat{T}_{ab}$ and $\hat{P}_{ab}$ indicate the direction in which the incident wave impinges upon the interface. As shown in Figure 4.3 the incident wave is in medium "a" for the preceeding result. To consider a wave incident in "b" the subscripts of the coeffieients and the impedances simply need to be changed.

A-2 Impedance in Terms of Optical Parameters

It is possible to express $\hat{Z}$ in terms of $\hat{n}$ in order to rewrite equations (4-5) and (4-6) in terms of the

variables of the model, $\hat{n}_0$ $\hat{n}_1$ and $\hat{n}_2$. Using equation (4-3) we can write for propagation in the z direction

$$d\hat{E}_x/dz = -(\mu/c)\, d\hat{H}_y/dt \quad . \tag{A-15}$$

$\hat{E}_x$ has been set forth in equation (4-4). $\hat{H}_y$ has the same form but is out of phase with $\hat{E}_x$ by Ψ, see Figure 4.3,

$$\hat{H}_y = H_0\, e^{i\omega(t - \hat{n}z/c - \Psi/\omega)} \quad . \tag{A-16}$$

From the definition of impedance,

$$\hat{Z} = \hat{E}_x / \hat{H}_y \tag{A-17}$$

which yields,

$$\hat{Z} = E_0/H_0\, e^{i\Psi} \quad . \tag{A-18}$$

By differentiating (4-4) and (A-16) one obtains

$$d\hat{E}_x/dz = -E_0\, i\omega\hat{n}/c \quad e^{i\omega(t - \hat{n}z/c)} \tag{A-19}$$

and

$$d\hat{H}_y/dt = H_0\, i\omega \quad e^{i\omega(t - \hat{n}z/c - \Psi/\omega)} \quad . \tag{A-20}$$

Substituting (A-19) and (A-20) into (A-15) yields

$$-E_0\, i\omega \hat{n}/c \;\; e^{i\omega(t - \hat{n}z/c)} =$$

$$-(\mu/c)\, H_0\, i\omega\, e^{i\omega(t - \hat{n}z/c - \Psi/\omega)}. \quad \text{(A-21)}$$

Solving for E_0 gives

$$E_0 = \mu H_0 \, (e^{-i\Psi})/\hat{n} \quad . \quad \text{(A-22)}$$

Substituting (A-22) into (A-18) yields

$$\hat{Z} = \mu / \hat{n} \quad . \quad \text{(A-23)}$$

The notation for the specific case may be modified to refer to medium "a",

$$\hat{Z}_a = \mu_a / \hat{n}_a \quad \text{(A-24)}$$

A-3 Attenuation Coefficients

The expression of the attenuation of the electric field strength of a propagating electromagnetic wave as it passes through an absorbing medium may be found as follows. Consider equation (4-4) and set z = 0, then

$$\hat{E}_{x1} = E_0 \, e^{i\omega t} \quad . \quad \text{(A-25)}$$

Setting z = d expresses the electric field strength at "d" distance into the medium,

$$\hat{E}_{x2} = E_0 \, e^{i\omega(t - \hat{n}d/c)} \quad . \tag{A-26}$$

Let

$$\hat{A} = \hat{E}_{x2} \; / \; \hat{E}_{x1} \tag{A-27}$$

which yields

$$\hat{A} = e^{-i\omega\hat{n}d/c} \quad . \tag{A-28}$$

A-4 Simplification of the Master Equation

Consider the master equation of the model,

$$\frac{\Delta R}{\bar{R}} = 2\frac{\left|\hat{P}_{01}\hat{T}_{01}\hat{A}_{d1}^2\hat{P}_{12}\hat{T}_{10}\right|^2 - \left|\hat{P}_{01}\hat{T}_{01}\hat{A}_{d2}^2\hat{P}_{12}\hat{T}_{10}\right|^2}{\left|\hat{P}_{01}\hat{T}_{01}\hat{A}_{d1}^2\hat{P}_{12}\hat{T}_{10}\right|^2 + \left|\hat{P}_{01}\hat{T}_{01}\hat{A}_{d2}^2\hat{P}_{12}\hat{T}_{10}\right|^2} \quad . \tag{4-22}$$

Let

$$\hat{P}_{01} = a \, e^{i\theta_a} \tag{A-29}$$

and

$$\hat{T}_{01}\hat{A}_{d1}^2\hat{P}_{12}\hat{T}_{10} = b \, e^{i\theta_b} \quad . \tag{A-30}$$

Rearranging (4-19) and substituting (A-29) and (A-30)

$$\left|\hat{E}_1 \; / \; \hat{E}_i\right|^2 = \left|\hat{P}_{01}\hat{T}_{01}\hat{A}_{d1}^2\hat{P}_{12}\hat{T}_{10}\right|^2 = \left|a \, e^{i\theta_a} + b \, e^{i\theta_b}\right|^2$$

Because $xe^{iy} = x (\cos y + i \sin y)$

$$\left|E_1/E_i\right|^2 = a(\cos\theta_a + i \sin\theta_a) + b(\cos\theta_b + i \sin\theta_b)^2 .$$

Combining the real and imaginary parts,

$$\left|E_1/E_i\right|^2 = a\cos\theta_a + b\cos\theta_b + i(a\sin\theta_a + b\sin\theta_b)^2 .$$

Because $\left|X + iY\right| = (X^2 + Y^2)^{\frac{1}{2}}$,

$$\left|E_1/E_i\right|^2 = (a\cos\theta_a + b\cos\theta_b)^2 + (a\sin\theta_a + b\sin\theta_b)^2 .$$

Expanding the terms,

$$\left|E_1/E_i\right|^2 = a^2(\cos^2\theta_a + \sin^2\theta_a) + b^2(\cos^2\theta_b + \sin^2\theta_b) +$$

$$2ab(\cos\theta_a \cos\theta_b + \sin\theta_a \sin\theta_b) .$$

Applying trigonometric identies,

$$\left|E_1/E_i\right|^2 = a^2 + b^2 + 2ab \tfrac{1}{2}(\cos(\theta_a + \theta_b) + \cos(\theta_a - \theta_b) -$$

$$\cos(\theta_a + \theta_b) + \cos(\theta_a - \theta_b)) .$$

Combining terms yields

$$\left|E_1/E_i\right|^2 = a^2 + b^2 + 2ab \cos(\theta_a - \theta_b) \quad . \qquad \text{(A-31)}$$

Because $\hat{A}_{d1}$ and $\hat{A}_{d2}$ have wavelength dependence, this fact needs to be shown explicitly. From equation (4-17)

$$\hat{A}_{d1}\,\hat{A}_{d1} = \hat{A}_{d1}^2 = e^{-i2\omega\hat{n}_1 d_1/c} \quad . \qquad \text{(A-32)}$$

In order to express the wavelength dependence in (A-31) let

$$b\, e^{i\theta_b} = f\, e^{i\theta_f}\, \hat{A}_{d1}\, \hat{A}_{d1} \quad .$$

Substituting (A-32)

$$b\, e^{i\theta_b} = f\, e^{i\theta_f}\, e^{-i2\omega n_1 d_1/c} \quad .$$

Because $\hat{n}_1 = n_1 - i\,k_1$,

$$b\, e^{i\theta_b} = f\, e^{i\theta_f}\, e^{-2\omega k_1 d_1/c}\; e^{-i2\omega n_1 d_1/c} \quad .$$

Combining terms,

$$b\, e^{i\theta_b} = f\, e^{-2\omega k_1 d_1/c}\; e^{i(\theta_f - 2\omega n_1 d_1/c)} \quad . \qquad \text{(A-33)}$$

From the magnitude and phase of (A-33)

$$b = f\, e^{-2\omega k_1 d_1/c} \tag{A-34}$$

and

$$\theta_b = (\theta_f - 2\omega n_1 d_1/c) \quad . \tag{A-35}$$

Substituting (A-34) and (A-35) into (A-31) yields

$$|E_1/E_i|^2 = a^2 + f^2\, e^{-4\omega k_1 d_1/c} + 2af\, e^{-2\omega k_1 d_1/c} \cos(\varphi + 2\omega n_1 d_1/c) \quad . \tag{A-36}$$

Where from equations (A-29), (A-30) and (A-33),

$$a = |\hat{P}_{01}| \quad , \tag{A-37}$$

$$f = |\hat{T}_{01}\hat{P}_{12}\hat{T}_{10}| \tag{A-38}$$

and

$$\varphi = \theta_a - \theta_f = \tan^{-1}\frac{\text{Imag}(\hat{P}_{01})}{\text{Real}(\hat{P}_{01})} - \tan^{-1}\frac{\text{Imag}(\hat{T}_{01}\hat{P}_{12}\hat{T}_{10})}{\text{Real}(\hat{T}_{01}\hat{P}_{12}\hat{T}_{10})} \quad . \tag{A-39}$$

The exponential terms are normally very close to unity for equation (A-36) in the case of a dielectric medium. For the purposes of visualization the following derivation shows when the exponentials of (A-36) may be considered to be virtually unity. Observe

$$e^{-2\omega k_1 d_1/c} \gg e^{-4\omega k_1 d_1/c} \quad . \tag{A-40}$$

Let the maximum error be E

$$1 - e^{-2\ k_1 d_1/c} < E \quad . \tag{A-41}$$

Solving leads to

$$k_1 d_1/\lambda < -\ln(1 - E)/4\pi \quad . \tag{A-42}$$

The following is an example using equation (A-42). The wavelength giving the largest error is the shortest occuring in the spectrum. Selecting the following values:

λ = 200 nanometers

$k_1 = 2 \times 10^{-6}$ (quartz)

E = .001 (this establishes a maximum error of 0.1%)

And solving (A-42) gives

$d_1 < 7950$ nm

This is a very large thickness. The oxide films produced in this work are generally much thinner.[8] Of course

the restriction of (A-42) must be tested for each material to be assured of its applicability. Considering the exponentials to be unity yields

$$\left|E_1/E_i\right|^2 = a^2 + f^2 + 2af\cos(\varphi + 2\omega n_1 d_1/c) \quad . \qquad \text{(A-43)}$$

Similarly

$$\left|E_2/E_i\right|^2 = a^2 + f^2 + 2af\cos(\varphi + 2\omega n_1 d_2/c) \quad . \qquad \text{(A-44)}$$

Now combining (A-43),(A-44) and (4-21)

$$\Delta R/\bar{R} =$$

$$\frac{a^2+f^2+2af\cos(\varphi+2\omega n_1 d_1/c)-a_2-f_2-2af\cos(\varphi+2\omega n_1 d_2/c)}{2\,a^2+f^2+2af\cos(\varphi+2\omega n_1 d_1/c)+a^2+f^2+2af\cos(\varphi+2\omega n_1 d_2/c)}$$

$$= \frac{4af(\cos(\varphi+2\omega n_2 d_1/c)-\cos(\varphi+2\omega n_1 d_2/c))}{2a^2+2f^2+2af\cos(\varphi+2\omega n_1 d_1/c)+\cos(\varphi+2\omega n_1 d_2/c)} \cdot \qquad \text{(A-45)}$$

Consider the numerator of (A-45),

$$N = \cos(\varphi + 2\omega n_1 d_1/c) - \cos(\varphi + 2\omega n_1 d_2/c) \quad .$$

Because $\cos(x + y) = \cos x \cos y - \sin x \sin y$,

$$N = \cos\varphi\cos(2\omega n_1 d_1/c) - \sin\varphi\sin(2\omega n_1 d_1/c) -$$
$$\cos\varphi\cos(2\omega n_1 d_2/c) + \sin\varphi\sin(2\omega n_1 d_2/c) \quad .$$

Combining terms,

$$N = \cos\varphi\ (\cos(2\omega n_1 d_1/c)-\cos(2\omega n_1 d_2/c)) - \sin\varphi\ (\sin(2\omega n_1 d_1/c)-\sin(2\omega n_1 d_2/c)) .$$

Applying trigonometric identies,

$$N = \cos\varphi\ (-2\sin(\omega n_1(d_1+d_2)/c)\ \sin(\omega n_1(d_1-d_2)/c)) - \sin\varphi\ (\ 2\cos(\omega n_1(d_1+d_2)/c)\ \sin(\omega n_1(d_1-d_2)/c)).$$

Combining terms,

$$N = -2\ \sin(\omega n_1(d_1-d_2)/c)(\cos\varphi\ \sin(\omega n_1(d_1+d_2)/c) + \sin\varphi\ \cos(\omega n_1(d_1-d_2)/c)) .$$

Applying trigonometric identies,

$$N = -2\sin(\omega n_1(d_1-d_2)/c)\ \sin(\varphi+\omega n_1(d_1+d_2)/c) . \qquad \text{(A-46)}$$

Similarly the denominator equals,

$$D = a^2+f^2+2af\ \cos(\omega n_1(d_1-d_2)/c)\ \cos(\varphi+ n_1(d_1+d_2)/c). \qquad \text{(A-47)}$$

Combining the numerator and denominator terms,

$$\Delta R/\ \overline{R} = \frac{4af\ \sin(\omega n_1(d_1-d_2)/c)\ \sin(\varphi+\omega n_1(d_1+d_2)/c)}{a^2+f^2+2af\ \cos(\omega n_1(d_1-d_2)/c)\ \sin(\varphi+\omega n_1(d_1+d_2)/c)} \qquad \text{(A-48)}$$

Rearranging and considering (4-23) yields

$$\frac{\Delta R}{\bar{R}} = \frac{2 \sin(2\pi n_1(d_1-d_2)/\lambda) \sin(\Phi + 2\pi n_1(d_1+d_2)/\lambda)}{g+\cos(2\pi n_1(d_1-d_2)/\lambda) \cos(\Phi + 2\pi n_1(d_1+d_2)/\lambda)} .$$

(A-49)

APPENDIX B
MULTIPLE INTERNAL REFLECTION EQUATION

B-1 Derivation of the Equation

The derivations and equations in the text of this dissertation assume a single internal reflection when light impinges on a thin oxide film covering a metal substrate. This assumption introduces little error under many experimental conditions and it leads to equations which are easier to comprehend than those which account for multiple internal reflections. However, employing the multiple internal reflection equation allows more accurate results.

Figure B.1 shows the path of a multiply reflected ray of light which initially impinges upon the thin oxide film at the upper left of the figure. The electric field, $\hat{E}$, of each emerging ray may be related to the incident electric field in a way paralleling the method described in subsection IV-3 in the text. The first component, $\hat{E}_1$, results from the reflection at the 0-1 interface.

$$\hat{E}_1 = \hat{E}_i \hat{P}_{01} \qquad \text{(B-1)}$$

The $\hat{E}_2$ component results from the transmission of the incident ray ($\hat{T}_{01}$) followed by an absorption term ($\hat{A}$),

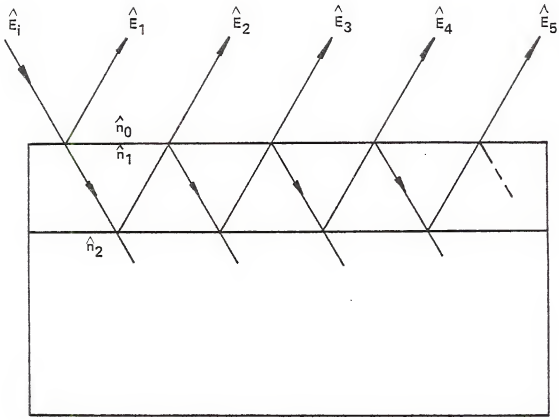

Figure B.1 Interactions between a light beam, $\hat{E}_i$, and a solid consisting of a semi-transparent medium of optical index, $\hat{n}_1$ and an absorbing substrate of index $\hat{n}_2$. The solid is surrounded by a medium of index $\hat{n}_0$. For clarity the incident and reflected rays are shown at an angle, the calculation is carried out at normal incidence.

reflection from the 1-2 interface ($\hat{P}_{12}$), another absorption ($\hat{A}$) and transmission through the 0-1 interface ($\hat{T}_{10}$).

$$\hat{E}_2 = \hat{E}_i \hat{T}_{01} \hat{A}^2 \hat{P}_{12} \hat{T}_{10} \quad . \tag{B-2}$$

Similarly $\hat{E}_3$ may be found,

$$\hat{E}_3 = \hat{E}_i \hat{T}_{01} \hat{A}^2 \hat{P}_{12} \hat{P}_{10} \hat{A}^2 \hat{P}_{12} \hat{T}_{10} \quad . \tag{B-3}$$

Substitution of (B-2) into (B-3) yields

$$\hat{E}_3 = \hat{E}_2 \hat{P}_{10} \hat{A}^2 \hat{P}_{12} \quad . \tag{B-4}$$

And in general,

$$\hat{E}_{n+1} = \hat{E}_n \hat{P}_{10} \hat{A}^2 \hat{P}_{12} \quad , n = 2, 3, 4, \ldots \quad . \tag{B-5}$$

Allowing

$$\hat{X} = \hat{P}_{10} \hat{A}^2 \hat{P}_{12} \quad , \tag{B-6}$$

and substituting (B-6) into (B-5) yields

$$\hat{E}_{n+1} = \hat{E}_n \hat{X} \quad , \quad n = 2, 3, 4, \ldots \quad . \tag{B-7}$$

It follows that

$$\hat{E}_{n+m} = \hat{E}_n \hat{X}^m \quad , \quad n = 2, 3, 4, \ldots , \quad m = 1, 2, \ldots \quad \text{(B-8)}$$

The sum of the reflected electric fields of the electromagnetic waves may be written as follows:

$$\hat{E}_T = \hat{E}_1 + \hat{E}_2 + \hat{E}_3 + \hat{E}_4 + \hat{E}_5 + \ldots \quad \text{(B-9)}$$

Substituting (B-8) into (B-9) yields

$$\hat{E}_T = \hat{E}_1 + \hat{E}_2 \left(1 + \hat{X} + \hat{X}^2 + \hat{X}^3 + \ldots \right) \quad . \quad \text{(B-10)}$$

If $\left|\hat{X}\right|$ is less than one,

$$1 + \hat{X} + \hat{X}^2 + \hat{X}^3 + \hat{X}^4 + \ldots = 1/(1 - \hat{X}) \quad . \quad \text{(B-11)}$$

Substituting (B-11) into (B-10),

$$\hat{E}_T = \hat{E}_1 + \hat{E}_2 \; / \; (1 - \hat{X}) \quad . \quad \text{(B-12)}$$

Inserting (B-1), (B-2) and (B-6) into (B-12) yields the total reflected electric field, $\hat{E}_T$, in terms of the incident field, $\hat{E}_i$, and the coefficients defined in subsection IV-3 which are functions of the materials properties of the media.

$$\hat{E}_T = \hat{E}_i\hat{P}_{01} + \hat{E}_i\hat{T}_{01}\hat{A}^2\hat{P}_{12}\hat{T}_{10} \,/\, (1 - \hat{P}_{10}\hat{A}^2\hat{P}_{12}) \quad .(B\text{-}13)$$

Referring the equation (B-13) to the specific thicknesses of the two oxide films as shown in Figure 4.1 we obtain

$$\hat{E}_{d1} = \hat{E}_i(\hat{P}_{01} + \hat{T}_{01}\hat{A}^2_{d1}\hat{P}_{12}\hat{T}_{10} \,/(1-\hat{P}_{10}\hat{A}^2_{d1}\hat{P}_{12})) \quad (B\text{-}14)$$

and

$$\hat{E}_{d2} = \hat{E}_i(\hat{P}_{01} + \hat{T}_{01}\hat{A}^2_{d2}\hat{P}_{12}\hat{T}_{10} \,/(1-\hat{P}_{10}\hat{A}^2_{d2}\hat{P}_{12})) \quad , (B\text{-}15)$$

Substituting (B-14) and (B-15) into (4-21) yields the master equation for $\Delta R/\bar{R}$.

$$\Delta R/\bar{R} =$$

$$2\,\frac{\left|\hat{P}_{01} + \dfrac{\hat{T}_{01}\hat{A}^2_{d1}\hat{P}_{12}\hat{T}_{10}}{1 - \hat{P}_{10}\hat{A}^2_{d1}\hat{P}_{12}}\right|^2 - \left|\hat{P}_{01} + \dfrac{\hat{T}_{01}\hat{A}^2_{d2}\hat{P}_{12}\hat{T}_{10}}{1 - \hat{P}_{10}\hat{A}^2_{d2}\hat{P}_{12}}\right|^2}{\left|\hat{P}_{01} + \dfrac{\hat{T}_{01}\hat{A}^2_{d1}\hat{P}_{12}\hat{T}_{10}}{1 - \hat{P}_{10}\hat{A}^2_{d1}\hat{P}_{12}}\right|^2 + \left|\hat{P}_{01} + \dfrac{\hat{T}_{01}\hat{A}^2_{d2}\hat{P}_{12}\hat{T}_{10}}{1 - \hat{P}_{10}\hat{A}^2_{d2}\hat{P}_{12}}\right|^2} \quad (B\text{-}16)$$

This equation was programmed to produce calculated differential reflectograms similar to those produced by the single reflection equation (4-22). The program for the multiple reflection equation is included in subsection B-3.

B-2 Comparison of Multiple and Single Reflection Models

Figure B.2 is a calculated differential reflectogram of a thin oxide film on a metal substrate produced by employing the multiple internal reflection equation (B-16). The optical parameters are listed on the figure and in the figure caption. It can be seen that there is good qualitative agreement between the curves of Figure B.2 and those of Figure 4.7 which have been calculated using the single internal reflection equation. It can also be seen that for quantitative evaluations, the more exact equation (B-16) must be used.

B-3 Multiple Internal Reflection Computer Program

The program for multiple internal reflections is identical to the single internal reflection program listed in Appendix D, with the exception of the following statements.

```
R1=(CABS(P01+(T01*P12*T10*AT1*AT1)/(1.-P10*AT1*AT1*P12)))**2
```

and

```
R2=(CABS(P01+(T01*P12*T10*AT2*AT2)/(1.-P10*AT2*AT2*P12)))**2.
```

These statements replace the "R1" and "R2" statements in the single reflection program.

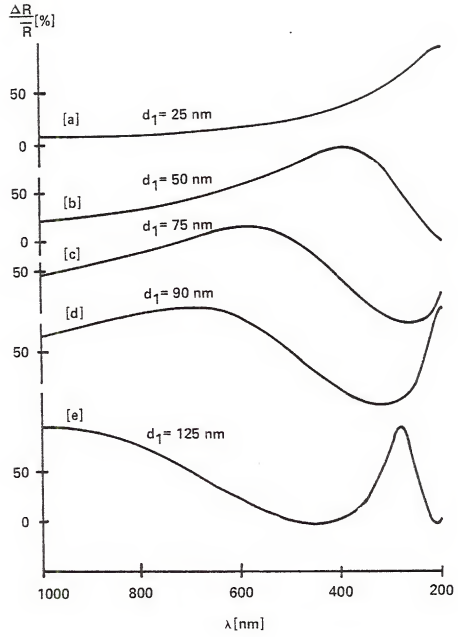

Figure B.2 Calculated differential reflectograms of a metal oxide on a metal substrate. The sample configuration is shown in Figure 4.1. The value of d_1 increases from curve (a) through (e) and d_2 is 0.1 nm. The values of the optical constants were taken to be $\hat{n}_0 = 1$, $\hat{n}_1 = 1.6 - i\ 2 \times 10^{-6}$ and $\hat{n}_2 = 3 - i\ 3$.

APPENDIX C
DIFFERENCE IN THICKNESS

Reduction in the difference in thickness of the two thin corrosion product films can have two distinct effects on the differential reflectograms. If g is close to unity, the peaks will sharpen as shown in subsection IV-6. If g is not close to unity, the peak heights will be reduced as the difference in thickness is reduced. The first case is that in which g is not close to unity. Inspection of equation (4-24) reveals that a peak in the spectrum can be obtained in a differential reflectogram if the following is true:

$$\sin(\varphi + 2\pi n_1(d_1 + d_2)/\lambda) = 1 \quad . \tag{C-1}$$

Simultaneously

$$\cos(\varphi + 2\pi n_1(d_1 + d_2)/\lambda) = 0 \quad . \tag{C-2}$$

Substituting (C-1) and (C-2) into (4-24) yields

$$\Delta R/\bar{R} = 2 \sin(2\pi n_1(d_1 - d_2)/\lambda)(1)/(g + 0). \tag{C-3}$$

Let the maximum in $\Delta R/\bar{R}$ be D, then

The value of g is not known beforehand so typical values must be selected. From equation (4-26) it can be seen that the largest value of g occurs when a or f is large. In the case of dielectric layers on absorbing substrates f will be larger than a. Thus typical extreme values are

$$a = 0.1 \qquad \text{(C-5)}$$

and

$$f = 0.9 \quad . \qquad \text{(C-6)}$$

Therefore

$$g = 4 \quad . \qquad \text{(C-7)}$$

Substituting (C-7) into (C-3) yields

$$n_1(d_1 - d_2)/\lambda \; < \; (1/2\pi) \sin^{-1}(2D) \quad . \qquad \text{(C-8)}$$

Let

$$F = (1/2\pi) \sin^{-1}(2D) \quad . \qquad \text{(C-9)}$$

Combining (C-8) and (C-9) yields

$$n_1(d_1 - d_2)/\lambda \; < \; F \quad . \qquad \text{(C-10)}$$

Equation (C-10) indicates that F increases when n_1 and/or $(d_1 - d_2)$ increases and when λ decreases.

The application of (C-10) can be demonstrated by an example. Assume it is desired to limit the maximum peak height for interference peaks to 10% (0.1). Letting D = 0.1 in (C-9) gives

$$F = 3.20 \times 10^{-2} \quad . \tag{C-11}$$

Substituting (C-11) into (C-10) for λ = 200 nm yields

$$n_1(d_1 - d_2) < 6.4 \text{ nm} \quad . \tag{C-12}$$

Thus the condition under which interference peaks in the example will be below 10% is a low $n_1 \times (d_1 - d_2)$ product as shown in (C-12)

In Figure C.1, calculated differential reflectograms are presented for the sample configuration of Figure 4.1. The value of n_1 is varied from curve (a) to curve (f) as shown in the figure. Other parameters are in the figure caption. It can be seen that the maximum peak height increases with n_1 in accordance with (C-9) and (C-10). Curve (d) however, does not follow the trend because it violates the assumptions of (C-1) through (C-3) which presumed that the peaks come from a maximum in the numerator and a minimum in the denominator cosine product term.

Figure C.1 Calculated differential reflectograms of a metal oxide on a metal substrate. The sample configuration is shown in Figure 4.1. The value of n_1 is varied from curve (a) through (f). The optical constants were taken to be, $\hat{n}_0 = 1$, $k_1 = 2 \times 10^{-6}$ and $\hat{n}_2 = 3 - i\,3$. The thicknesses were $d_1 = 50$ nm and $d_2 = 49$ nm.

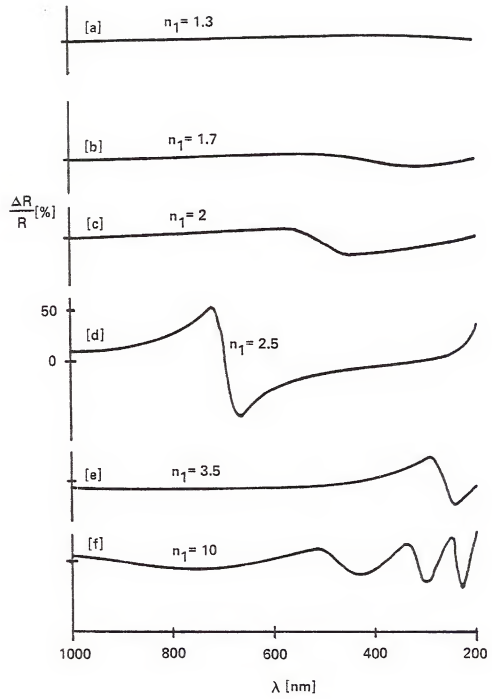
[a]
n_1= 1.3
[b]
n_1= 1.7
$\frac{\Delta R}{R}$[%]
[c]
n_1= 2
50
[d]
n_1= 2.5
0
[e]
n_1= 3.5
[f]
n_1= 10
1000
800
600
400
200
λ [nm]

As previously described in subsection IV-6, when g is nearly unity, the denominator of (4-24) may periodically go very close to zero as a function of wavelength. Figure C.1 shows that when g is nearly unity, the conditions of equation (C-4) break down because the peaks are coming solely from minima in the denominator.

In Figure C.2, calculated differential reflectograms are presented for the configuration of Figure 4.1. The value of d_1 is 50 nm while d_2 varies as shown in the figure. Other parameters are in the figure caption. The value of g is near unity. It can be seen that the value of the peak height is reduced as the value of $(d_1 - d_2)$ is reduced. Conclusions for these effects of $(d_1 - d_2)$ are presented in Table 4.1. The general effect is to clamp the maximum amplitude in the differential reflectogram.

Figure C.2 Calculated differential reflectograms of a metal oxide on a metal substrate. The thickness of the oxide on the two specimen halves is different and is indicated on the figure. Also see Figure 4.1 for the theoretical configuration. For the calculations the optical constants were taken to be $\hat{n}_0 = 1$, $\hat{n}_1 = 2.5 - i\ 2 \times 10^{-6}$ and $\hat{n}_2 = 3 - i\ 3$.

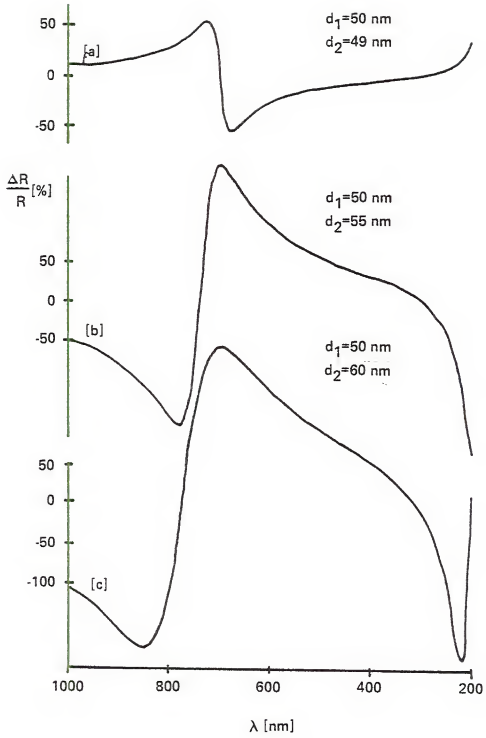
50
0
-50
[a]
d1=50 nm
d2=49 nm
ΔR/R [%]
50
0
-50
[b]
d1=50 nm
d2=55 nm
d1=50 nm
d2=60 nm
50
0
-50
-100
[c]
1000
800
600
400
200
λ [nm]

APPENDIX D
SINGLE INTERNAL REFLECTION PROGRAM

```
      COMPLEX N0,N1,N2,P01,T10,P12,AT1,AT2,T01,ARG1,ARG2,N10
      DIMENSION RDEL(803),WVL(803),A(10),WL(10),S(10)
      PI=3.1415926535
      C=3.E8
    1 READ(5,100) IN,IT,IA,NP,ND
  100 FORMAT(3I1,2I2)
      IF(IN.EQ.0) READ(5,101)N0,N1,N2
  101 FORMAT(3F10.4,F10.8,2F10.4)
      N10=N1
      IF(IT.EQ.0) READ(5,102)T1N,T2N
  102 FORMAT(2F10.4)
      IF(IA.GT.0) GO TO 5
      DO 2 I=1,NP
      READ(5,103) A(I),WL(I),S(I)
  103 FORMAT(3F10.4)
    2 CONTINUE
    5 WRITE(6,200)N0,N1,N2
  200 FORMAT('  N0= ',2G15.5,'  N1 =',2G15.5,'  N2= ',2G15.5)
      WRITE(6,201) T1N,T2N
  201 FORMAT('0 T1=',F10.4,'NANOMETERS  T2=',F10.4,'NM')
      IF(IT.EQ.0) T1=T1N*1.E-9
      IF(IT.EQ.0) T2=T2N*1.E-9
```

```
      DO 3 L=1,801
      WVL(L)=199+L
      N1=N10
      DO 4 J=1,NP
      FAC=-.5*((WVL(L)-WL(J))/S(J))**2
      IF(FAC.LT.-50.) FAC=-50.
      N1=N1+N1*A(J)*EXP(FAC)
    4 CONTINUE
      P01=(N0-N1)/(N0+N1)
      T01=2.*N0/(N0+N1)
      T10=2.*N1/(N1+N0)
      P12=(N1-N2)/(N1+N2)
      W=2*PI*C/(WVL(L)*1.E-9)
      ARG1=(0.,-1.)*W*N1*T1/C
      IF(CABS(ARG1).GT.50.)ARG1=(-50.,-50.)
      AT1=CEXP(ARG1)
      ARG2=(0.,-1.)*W*N1*T2/C
      IF(CABS(ARG2).GT.50.)ARG2=(-50.,-50.)
      AT2=CEXP(ARG2)
      R1=(CABS(P01+T01*P12*T10*AT1*AT1))**2
      R2=(CABS(P01+T01*P12*T10*AT2*AT2))**2
      RDEL(L)=200.*(R1-R2)/(R1+R2)
    3 CONTINUE
      RDEL(800)=100.
      RDEL(801)=-100.
```

```
 CALL DOTPLT(WVL,RDEL,801,0,'WAVELENGTH IN NANOMETERS',
124,'(DELTA R) /(R AVG) 5',19)
 IF(ND.EQ.0) GO TO 1
 STOP
 END
```

APPENDIX E
PROGRAM FUNCTION

The equations of the model for multiple internal reflections are written into a Fortran computer program, see Appenxix B. The data expected by the program can take on various forms to facilitate the input procedure. The first card read contains three one-digit integers followed by two two-digit integers. If "IN" is zero the program expects the next card to contain "N0", "N1" and "N2". If "IN" is one, the program uses the previous values for these parameters. For at least the first calculated reflectogram these parameters must be provided. If "IT" is zero, values of "T1N" and "T2N" will be expected on the following card. The "T1N" corresponds to d_1 and "T2N" is d_2. If "IT" is one, previous values are employed. Again at least the first calculation must be provided with these values. If "IA" is zero, values of "A(I)", "WL(I)" and "S(I)" will be expected on the next card. These values were allowed for and not used in these programs but the read instruction has been left in anticipating possible uses.

If "IA" is one , previous values would be used and as before, the initial calculation would require this card. The value of "NP" is unused. If the value of "ND" is zero, the program expects to calculate a reflectogram

and then return to the data file to calculate another reflectogram. When "ND" is one, the program calculates a final reflectogram corresponding to the data about to be read, then it terminates.

The next statements, up to number two, read in the data for the calculated reflectogram. It is important to observe the associated formats for this data. The following write statements print the data for each reflectogram to provide a record and to check that the data has been correctly read in.

The next statements, up to number three, calculate values of $\Delta R/\overline{R}$ from 200 to 1000 nanometers in wavelength at one nm increments. These values are placed in the array vectors "RDEL(L)" for $\Delta R/\overline{R}$ and "WVL(L)" for the wavelength.

The following two statements assign ficticious values to $\Delta R/\overline{R}$ at the 1000 nanometer end of the spectrum in order to obtain the same vertical scale on plots. The "CALL DOTPLT" statement delivers the calculated vectors to the plotting routine and the calculated differential reflectogram is automatically produced. After all data has been treated the program terminates.

The output consists of a series of pages containing the key data for one or more reflectograms. The following pages contain the actual calculated differential reflectograms. By use of the program, the effects of changes in the variables may be observed.

APPENDIX F
THICKNESS FROM PEAK POSITION

It is possible to calculate the thickness of an oxide film overlying a metal substrate if certain conditions are met. The oxide thickness on one sample half must be virtually zero. In addition the experimental reflectogram must contain at least three interference peaks. Other optical constants need not be known. From equation (4-38) it is possible to write the following because $d_2 = 0$.

$$\lambda_a = 2 n_1 d_1 / m_a \qquad \text{(F-1)}$$

The next peak in either direction comes from equation (4-39). The second peak from the first may be seen to satisfy,

$$\lambda_b = 2 n_1 d_1 / (m_a + 1) \quad . \qquad \text{(F-2)}$$

Solving (F-1) for m_a yields

$$m_a = 2 n_1 d_1 / \lambda_a \qquad \text{(F-3)}$$

and substituting into (F-2) and rearranging yields

$$\lambda_b (1 + 2 n_1 d_1 / \lambda_a) = 2 n_1 d_1 \quad . \qquad \text{(F-4)}$$

Solving leads to the equation:

$$d_1 = \frac{1}{2n_1} \quad \frac{\lambda_b \lambda_a}{\lambda_a - \lambda_b} \qquad \text{(F-5)}$$

A typical value for λ_a and λ_b can be seen in Figure 4.10.

REFERENCES

1. E. D. Verink, private communication

2. M. G. Fontana and N. D. Greene, Corrosion Engineering McGraw-Hill, New York (1967)

3. H. Kaesche, Passivity of Metals, R. P. Frankenthal and J. Kruger, Eds. Electrochemical Soc. Inc., Princeton, N. J., pp 935 - 959 (1978)

4. M. Metzger and J. Zahavi, Passivity of Metals, R. P. Frankenthal and J. Kruger, Eds. Electrochemical Soc. Inc., Princeton, N. J., pp 960 - 972 (1978)

5. N. Sato, Passivity of Metals, R. P. Frankenthal and J. Kruger, Eds. Electrochemical Soc. Inc., Princeton N. J. , pp 29 - 58 (1978)

6. A. Joshi, L. E. Davis and P. W. Palmberg, Methods of Surface Analysis, The American Elsevier Pub. Co., New York, pp 159 - 222 (1975)

7. W. M. Riggs and M. J. Parker, Methods of Surface Analysis, The American Elsevier Pub. Co., New York, pp 103 - 158 (1975)

8. C. W. Shanley, dissertation, University of Florida (1977)

9. H. E. Bennett and J. M. Bennett, Physics of Thin Films, Academic Press, New York, 4, 1 (1967)

10. J. M. Bennett and M. J. Booty, Appl. Opt. 5, 41 (1966)

11. J. M. Bennett and M. J. Booty, Appl. Opt. 8, 2366 (1969)

12. L. A. Catalán, J. Opt. Soc. Amer. 55, 857 (1965)

13. P. A. Flourny and W. J. Schaffers, Spectrochim Acta 22, 5 (1966)

14. W. N. Hansen, J. Opt. Soc. Amer. 63, 793 (1973)

15. H. M. Liddell, J. Phys. D: Appl. Phys. 7, 1588 (1974)

16. R. F. Miller and A. J. Taylor, J. Phys. D: Appl. Phys. 4, 1419 (1971)

17. P. O. Nilsson, Appl. Opt. 7, 435 (1968)

18. L. G. Schulz, Adv. Phys. 5, 102 (1957)

19. S. G. Tomlin, Britt. J. Appl. Phys. (J. Phys. D.), 1, 1667 (1968)

20. L. Tronstad, Trans. Farad. Soc. 29, 502 (1933)

21. C. W. Shanley, R. E. Hummel and E. D. Verink, Jr., Corr. Sci. 20, 467 (1980)

22. R. J. Nastasi-Andrews and R. E. Hummel, Phys. Stat. Sol. B. 88, 173 (1978)

23. A. Javan, Sci. Amer., 217, 239 (1967)

24. H. Ehrenreich, IEEE Spect. 2, 162 (1965)

25. S. Roberts, Phys. Rev. 100, 1667 (1955)

26. H. E. Bennett and W. F. Koehler, J. Opt. Soc. Amer. 50, 1 (1960)

27. J. E. Shaw and W. R. Blevin, J. Opt. Soc. Amer. 54, 334 (1964)

28. W. E. O. Neal and R. W. Fane, J. Phys. E. 6, 409 (1973)

29. P. N. Schatz, S. Maeda and K. Kozima, J. Chem. Phys. 38, 2658 (1963)

30. P. N. Schatz, S. Maeda, J. L. Hollenberg and D. A. Downs, J. Chem. Phys. 34, 175 (1961)

31. P. N. Schatz, J. Chem. Phys. 32, 894 (1960)

32. D. G. Avery, Proc. Phys. Soc. B., 65, 425 (1952)

33. A. H. Reed and E. Yeager, Appl. Opt. 7, 451 (1968)

34. A. Bagchi and A. H. Rajagopal, Sol. St. Com. 31, 127 (1979)

35. F. Abelès, Physics of Thin Films, Academic Press New York, 6, 151 (1971)

36. O. S. Heavens, Optical Properties of Thin Solid Films, Academic Press, New York, (1955)

37. L. Ward, A. Nag and L. C. W. Dixon, Britt. J. Appl. Phys. (J. Phys. D.), 2, 301 (1969)

38. F. Abelés and M. L. Théye, Surf. Sci. 5, 325 (1966)

39. S. Maeda, G. Thyagarajan, P. N. Schatz, J. Chem. Phys. 39, 3474 (1963)

40. G. Baldini and L. Rigaldi, J. Opt. Soc. Amer. 60, 495 (1970)

41. S. Y. Shieh, Phys. Lett. 29A, 46 (1969)

42. K. Kozima, W. Suëtaka, P. N. Schatz, J. Opt. Soc. Amer. 56, 181 (1966)

43. A. N. Saxena, J. Opt. Soc. Amer. 55, 1061 (1965)

44. F. A. Lucy, J. Chem. Phys. 16, 167 (1948)

45. D. W. Peterson and N. M. Bashara, J. Opt. Soc. Amer. 55, 845 (1965)

46. J. C. M. Garnett, Philos. Trans. R. Soc. London 203, 385 (1904)

47. V. K. Subashiev and A. A. Kukarskii, Phys. Stat. Sol. 23, 447 (1967)

48. K. Brudzewski, Thin Solid Films, 61, 183 (1979)

49. H. E. Bennett, D. K. Burge, R. L. Peck and J. M. Bennett, J. Opt. Soc. Amer. 59, 675 (1969)

50. J. M. Bennett and R. J. King, Appl. Opt. 9, 236 (1970)

51. D. W. Berreman, J. Opt. Soc. Amer. 60, 499 (1970)

52. W. Weinstein, Vacuum, 4, 3 (1954)

53. D. J. McAdam , Jr. and G. W. Geil, 23, 63 (1939)

54. A. T. Fromhold, Jr., Theory of Metal Oxidation, McGraw-Hill, New York, (1953)

55. M. A. K. L. Dissanayake and L. L. Chase, Phys. Rev. B. 18, 6872 (1978)

56. S. Sawada and G. C. Danielson, Phys. Rev. 113, 1008 (1959)

57. S. K. Deb, Phil. Mag. 27, 801 (1973)

58. S. K. Deb, Proc. Roy. Soc. A. 304, 211 (1968)

59. S. K. Deb and J. A. Chopoorian, J. Appl. Phys. 37, 4818 (1966)

60. L. L. Chase, Phys. Rev. B. 10, 2226 (1974)

61. R. Matz and H. Luth, Appl. Phys. 18, 123 (1979)

62. J. Aranovich, A. Ortiz and R. H. Bube, J. Vac. Sci. Technol. 16, 994 (1979)

63. S.Brahms and S. Nikitine, Sol. St. Comm. 3, 209 (1965)

64. A. Daunois, J. L. Deiss and S. Nikitine, Sol. St. Comm. 10, 649 (1972)

65. P. C. Ladelfe, A. W. Czanderna and J. R. Biegen, Thin Solid Films, 10, 403 (1972)

66. L. L. Y. Chang and B. Phillips, J. Amer. Cer. Soc. 52, 527 (1969)

67. R. J. Ackerman and E. G. Rauh, J. Phys. Chem. 67, 2596 (1963)

68. G. R. St. Pierre, W. T. Ebihara, M. J. Pool and R. Speiser, Trans. AIME, 224, 259 (1962)

69. L. Kopp, B. N. Harmon and S. H. Liu, Sol. St. Comm. 22, 677 (1977)

70. R. Enderlein, R. E. Hummel, J. B. Andrews, R. J. Nastasi-Andrews and C. W. Shanley, Phys. Stat. Sol. B. 88, 173 (1978)

71. J. D. Kraus, Electromagnetics, McGraw-Hill, New York (1953)

BIOGRAPHICAL SKETCH

Frank Karl Urban III was born July 29, 1947 in Dayton, Ohio. He attended The Ohio State University and earned a Bachelor of Science in Electrical Engineering degree in 1970. He immediately started graduate school at OSU but interrupted it to found Urban Marketing, Inc., a small, high technology advertizing agency. He returned to OSU in September of 1976 and completed a Master of Science in Biomedical Engineering in August 1977. He subsequently entered the Department of Materials Science and Engineering at the University of Florida in September of 1977 and has pursued the degree of Doctor of Philosophy since that date.

The author is a member of the Americal Institute of Mining, Metallurgical and Petroleum Engineers, The American Society for Metals, Alpha Sigma Mu, The American Ceramic Society, Keramos, The Institute of Electrical and Electronic Engineers, Eta Kappa Nu, the National Association of Corrosion Engineers and the Society of Plastic Engineers.

I certify that I have read this study and that in my opinion it conforms to acceptable standards of scholarly presentation and is fully adequate, in scope and quality, as a dissertation for the degree of Doctor of Philosophy.

Rolf E. Hummel, Chairman
Professor of Materials Science
and Engineering

I certify that I have read this study and that in my opinion it conforms to acceptable standards of scholarly presentation and is fully adequate, in scope and quality, as a dissertation for the degree of Doctor of Philosophy.

Ellis D. Verink, Jr.
Professor and Chairman of Materials
Science and Engineering

I certify that I have read this study and that in my opinion it conforms to acceptable standards of scholarly presentation and is fully adequate, in scope and quality, as a dissertation for the degree of Doctor of Philosophy.

Robert T. DeHoff
Professor of Materials Science
and Engineering

I certify that I have read this study and that in my opinion it conforms to acceptable standards of scholarly presentation and is fully adequate, in scope and quality, as a dissertation for the degree of Doctor of Philosophy.

John R. Ambrose
Professor of Materials Science
and Engineering

I certify that I have read this study and that in my opinion it conforms to acceptable standards of scholarly presentation and is fully adequate, in scope and quality, as a dissertation for the degree of Doctor of Philosophy.

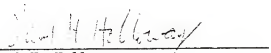

Paul H. Holloway
Associate Professor of Materials
Science and Engineering

I certify that I have read this study and that in my opinion it conforms to acceptable standards of scholarly presentation and is fully adequate, in scope and quality, as a dissertation for the degree of Doctor of Philosophy.

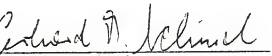

Gerhard M. Schmid
Associate Professor and Assistant
Chairman of Chemistry

This dissertation was submitted to the Graduate Faculty of the College of Engineering and to the Graduate Council, and was accepted as partial fulfillment of the requirements for the degree of Doctor of Philosophy.

March 1981

Herbert A. Lewis
Dean, College of Engineering

Dean for Graduate Studies and Research